

# Dynamics of monotone travelling fronts for discretizations of Nagumo PDEs

Christopher E Elmer<sup>1</sup> and Erik S Van Vleck<sup>2</sup>

<sup>1</sup> Department of Mathematical Sciences, New Jersey Institute of Technology, Newark, NJ 07102, USA

<sup>2</sup> Department of Mathematics, University of Kansas, Lawrence, KS 66045, USA

E-mail: elmer@oak.njit.edu and evanvleck@math.ku.edu

Received 12 August 2004, in final form 13 March 2005

Published 29 April 2005

Online at [stacks.iop.org/Non/18/1605](http://stacks.iop.org/Non/18/1605)

Recommended by Weinan E

## Abstract

When PDEs are discretized, the dynamics of the resulting equations differ from those of the original PDE. In this paper, we study the dynamics of travelling wave solutions to the discretized Nagumo PDE ( $A(\alpha)$  stable in time and/or uniform in space) with smooth bistable nonlinearities. In general, time discretization significantly speeds up travelling wave fronts and spatial discretization slows (or even halts) such fronts.

Mathematics Subject Classification: 35K57, 73D99, 65L, 65M

## 1. Introduction

Bistable reaction diffusion equations are used as modelling tools throughout the physical sciences, in fields varying from the study of the movement of solidification fronts in materials science to the propagation of action potential in neuroscience [5, 14, 21, 25, 27, 31, 32]. When solving, these equations are often discretized and studied numerically. In this paper, we illustrate the dynamics associated with the solution behaviour for the discretized equations, which is not present in the original reaction diffusion system. We focus entirely on travelling wave solutions for the Nagumo PDE [25]

$$u_t = \epsilon^2 \Delta u - f(u, \lambda), \quad (1)$$

where

- $u \equiv u(x, t)$ , where  $x \in \mathbb{R}^n$  for  $n = 1, 2$  or  $3$  and  $t \geq 0$ ,
- $\Delta$  is the standard Laplacian operator and

- $f$  is any smooth bistable nonlinearity with three zeros  $u_-(\lambda) \leq u_0(\lambda) \leq u_+(\lambda)$  (with at most one equality), which depend on a parameter  $\lambda$ , such that

$$f'(u_{\pm}) > 0, \quad f'(u_0) < 0 \quad (\text{except when } f'(u_+ = u_0) = 0, \quad f'(u_- = u_0) = 0)$$

$$\text{and} \quad \left| \int_{u_-}^{u_+} f(v) \, dv \right| < \infty. \quad (2)$$

As an illustrative example consider the cubic nonlinearity with  $\lambda$  set equal to the ‘detuning parameter’  $a$ :

$$f_{\text{cubic}}(u, a) \equiv u(u - a)(u - 1), \quad (3)$$

where

$$\begin{array}{llll} u_-(a) = a, & u_0(a) = 0, & u_+(a) = 1, & a \leq 0, \\ u_-(a) = 0, & u_0(a) = a, & u_+(a) = 1, & 0 < a < 1, \\ u_-(a) = 0, & u_0(a) = 1, & u_+(a) = a, & a \geq 1. \end{array}$$

Our contribution in this paper is to consider the effect of discretization (both spatial and temporal) on the behaviour of travelling wave solutions to bistable PDEs with smooth nonlinearities (such as (1)). Our approach is to consider the resulting differential-difference equations (for a semi-discretization, i.e. time *or* space) or the resulting difference equations (for a complete discretization, i.e. *both* time *and* space), to apply a travelling wave ansatz, and then to analyse the resulting travelling wave equations. The techniques we employ combine the use of an asymptotic analysis, the implicit function theorem and variational methods. We show and categorize the fundamentally different solution characteristics and wave speed properties that these travelling wave equations exhibit when compared with the travelling wave equations of the PDE (1), to include:

- a shape change of the solution profile, to being step-like, which corresponds to lurching in the motion of the interface for either *time* or *space* discretization,
- a slowing down and even failure of the interface to propagate for *space* discretization,
- a speeding up of the wave for *time* discretization and
- nonuniqueness of the wave speed–solution profile pair for *complete* discretization.

We focus on the dynamics as characterized by the relationship between the parameter  $\lambda$  (‘ $a$ ’ for the cubic nonlinearity (3)) and the speed of propagation of the travelling wave,  $c$ , and find that the effects of spatial discretization are most evident for wave speeds  $|c| \approx 0$ , while the effects of temporal discretization are most evident for large wave speeds. Our results serve to benchmark the effect of such discretization and may provide insight when inferring the dynamics from simulations. In space, when approximating solutions to partial differential equations in a neighbourhood of travelling wave solutions, we consider finite differences (centred differences) and in time we consider  $A(\alpha)$  stable linear multistep methods, focusing on BDF methods, which are the stiffly stable methods implemented in such widely used codes as DASSL [28, 29] and LSODE [18].

There has been much work on the existence and stability of monotone travelling wave solutions of bistable reaction–diffusion PDEs, notably the work of Fife and McLeod [13] and Aronson and Weinberger [2]. Notable work related to time discretization includes that of Weinberger [31] and Chow *et al* [3] that considers (up to rescaling) a uniform in space, forward Euler in time complete discretization. In [3] it is shown that nontrivial travelling wave solutions of the spatially discrete Nagumo equation are asymptotically stable with asymptotic phase. Furthermore, in [3], for uniform in space, forward Euler in time complete discretizations the

existence of travelling waves for small time steps  $\Delta t > 0$  and their asymptotic stability is shown. The results in [3] apply to other time discretizations as well. In this paper, we consider the discretization in time with a class of *implicit* methods and focus on the dynamics as characterized by the relationship between the detuning parameter and the wave speed. These time discretizations are appropriate because they are  $A(\alpha)$  stable linear multistep methods, and because they are regular methods (see, e.g., [30]) that do not add or subtract equilibrium solutions. Work on travelling wave solutions of spatially discrete bistable equations has been motivated by the importance of these types of equations as models in their own right (see, e.g., [4, 8, 19–21, 33, 34]). The work of Mallet-Paret in [23, 24] provides a general means for establishing the existence and studying the global structure of travelling wave solutions of mixed type delay differential equations, characterized by the presence of both backward and forward delays—equations that occur when considering the travelling wave equations for such spatially discrete systems.

The outline of this paper is as follows. In section 2 we review some known results (like finite wave speed) for travelling wave solutions of Nagumo type PDEs and introduce the smooth bistable nonlinearities that will be used in the examples. In section 3 we explicitly define the temporal, spatial and complete discretizations and we define the resulting travelling wave equations for each of these cases. We consider  $A(\alpha)$  linear multistep methods based on backward differentiation formulae and a uniform finite difference spatial discretization. We also describe the numerical method used throughout this paper and the two-point boundary interval problem solver COLMTFDE that we have developed. Section 4 is a study of just the temporal discretization. It begins with a review of the main tool used in this section, the implicit function theorem, in particular the formulation due to MacKay and Sepulchre [22]. We then state and prove our main results for the behaviour of travelling wave solutions under temporal discretization (e.g. speed-up of the wave and unbounded wave speed for some values of  $\Delta t$ ) for the cubic and sine nonlinearities, and we discuss extensions to general smooth bistable nonlinearities. Section 5 is devoted to the behaviour of uniform spatial discretizations. We introduce the variational principle developed in [17] before presenting results for spatial discretizations, such as slowing down of the wave and even failure of the wave to propagate. In section 6 we combine the results on temporal and spatial discretization to provide a picture of the behaviour of complete discretizations, the main result being a certain nonuniqueness of possible solutions. Section 7 contains our conclusions.

## 2. Background: travelling waves for Nagumo-type PDEs

A travelling wave solution is a plane wave  $(\varphi, c)$  in  $\mathbb{R}^n$  satisfying the travelling wave ansatz  $\varphi(x \cdot \sigma - ct) = u(x, t)$  (where  $\sigma \in \mathbb{R}^n$  satisfies  $\|\sigma\|_2 = 1$  and specifies the direction in which the plane wave is propagating). The function  $\varphi$  determines the profile of the wave and  $c$  determines the wave speed. The so-called travelling wave equation that must be satisfied for (1) is

$$-c\dot{\varphi}(\xi) = \epsilon^2 \ddot{\varphi}(\xi) - f(\varphi(\xi), \lambda), \quad \xi = x \cdot \sigma - ct \in \mathbb{R}, \quad (4)$$

together with the boundary conditions at  $\xi = \pm\infty$ . Observe that the travelling wave equation (4) is independent of the dimension  $n$  and the direction of propagation  $\sigma$ . Uniqueness only occurs when  $u_- < u_0 < u_+$  and the wave connects the saddle nodes  $u_-$  and  $u_+$ , and then only up to translation.

**Example 2.1.**  $f_{\text{cubic}}$ . *The travelling wave solutions of (4) with cubic nonlinearity  $f_{\text{cubic}}$  (3) are fairly well known. For  $\lambda = a \in \mathbb{R}$  there exist three possible travelling wave solutions*

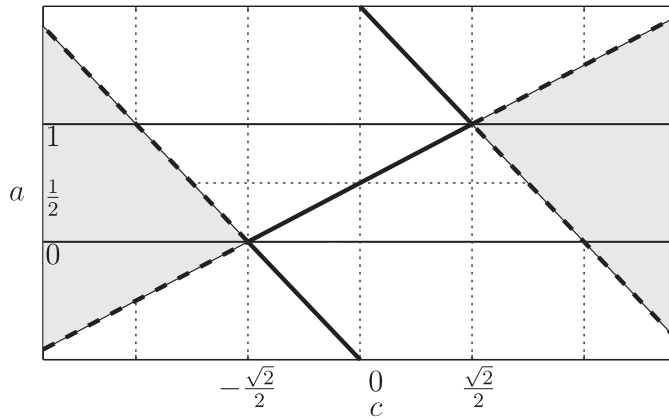


**Figure 1.** Plot of  $(a, c)$  curves for (4) with cubic nonlinearity (3). The thick solid lines are the  $(a, c)$  values for the stable heteroclinic orbits. The dashed lines are the boundaries of the regions (shaded areas) where  $(a, c)$  values are for Fisher type flows.

(mod symmetry), depending on which roots of  $f$  are involved in the flow (figure 1 illustrates the following). Letting  $\varphi(-\infty)$  and  $\varphi(\infty)$  be equal to any two of the three roots of  $f_{\text{cubic}}$  (0,  $a$  and 1) (for simplicity we chose  $\varphi(-\infty) \leq \varphi(\infty)$  here), all three solutions can be written as

$$\varphi_{u_1, u_3}(\xi) = \frac{1}{2} \left[ (u_1 + u_3) + (u_3 - u_1) \tanh \left( \frac{(u_3 - u_1)\xi}{2\epsilon\sqrt{2}} \right) \right] \tag{5}$$

with

$$c_{u_1, u_3} = \frac{\epsilon}{\sqrt{2}}(2u_2 - u_3 - u_1) \quad \text{and} \quad u_1 = \varphi(-\infty), \quad u_3 = \varphi(\infty)$$

and  $u_2$  is the third root of  $f_{\text{cubic}}$ . When  $u_2 \in (u_1, u_3)$  is fixed, the solution  $(\varphi_{u_1, u_3}, c_{u_1, u_3})$  is unique and globally stable. For  $u_2 \in (-\infty, u_1] \cup [u_3, \infty)$  fixed, the speed of the wave  $|c| \in [|c_{u_1, u_3}|, \infty)$  and  $\varphi_{u_1, u_3}$  is the profile for the minimum value of  $|c|$ ,  $|c_{u_1, u_3}|$ . Let  $b = \epsilon/\sqrt{2}$ , then, we have the following:

Connecting	$u_2 \in (u_1, u_3)$	$u_2 \in [u_3, \infty)$	$u_2 \in (-\infty, u_1]$
$u_1 = 0, u_3 = 1$	$a \in (0, 1), c_{0,1} \in (-b, b)$	$a \geq 1, c \in [c_{0,1}, \infty)$	$a \leq 0, c \in (-\infty, c_{0,1}]$
$u_1 = 0, u_3 = a$	$a > 1, c_{0,a} \in (-\infty, b)$	$a \leq 1, c \in [c_{0,a}, \infty)$	
$u_1 = a, u_3 = 1$	$a < 0, c_{a,1} \in (-b, \infty)$		$a \geq 0, c \in (-\infty, c_{a,1}]$

From this we see that the solution profile  $\varphi$  connecting  $u_-$  and  $u_+$  for (4) obtained when using the cubic nonlinearity with  $u_0 \in (u_-, u_+)$  does not depend on the wave speed  $c$  or the value of  $u_0$ . These travelling wave solutions are unique and stable to perturbations. For the case  $u_- < u_0 \leq u_+$  or  $u_- \leq u_0 < u_+$  we still have a heteroclinic orbit but now the solution profile changes with the wave speed  $c$  and  $a = u_0 = u_-$  or  $u_+$  is constant. Two of the three zeros of the cubic nonlinearity (3) have combined into one and travelling waves are now very much like those for the Fisher equation [14], a monostable PDE characterized by a quadratic reaction term/nonlinearity. These travelling waves become unstable to perturbations in the leading tails and become dependent on the initial profile. The wave speeds of the Fisher type solutions of (4) with  $f_{\text{cubic}}$  (3), where  $u_0 = a = 0$  or  $1$ , are always greater in magnitude than the speed of the travelling wave front connecting 0 and 1 with  $u_0 = a \in (0, 1)$ . In addition,

for  $a \in (0, 1)$   $|c_{0,1}| < |c_{0,a}|$  and  $|c_{a,1}|$ , i.e. the wave connecting 0 and 1 moves slower than the wave connecting 0 and  $a$  and the wave connecting  $a$  and 1.

Besides (3), other examples of nonlinearities that will be considered in this paper are for  $\delta \geq 0$ :

$$f_1(u) \equiv \begin{cases} u, & u < \frac{a}{(1+\delta)}, \\ \frac{1}{\delta}(a-u), & \frac{a}{(1+\delta)} \leq u \leq \frac{(a+\delta)}{(1+\delta)}, \\ u-1, & u > \frac{(a+\delta)}{(1+\delta)}, \end{cases} \tag{6}$$

where  $u_- = 0, u_0 = a$  and  $u_+ = 1$ ; and

$$f_2(u) \equiv \begin{cases} u, & u < a - \delta, \\ \frac{u^3 - 3u^2a + (3a^2 - 3\delta^2 + 4\delta^3)u - (2\delta^3 - 3a\delta^2 + a^3)}{4\delta^3}, & -\delta \leq u - a \leq \delta, \\ u - 1, & u < a + \delta, \end{cases} \tag{7}$$

where  $u_- = 0$  and  $u_+ = 1$ . Nonlinearities (7) and (6) converge pointwise to the McKean piecewise linear nonlinearity [27]

$$f_{\text{pwl}}(u, a) \equiv \begin{cases} u, & u < a, \\ [a - 1, a] & u = a, \\ u - 1, & u > a, \end{cases} \tag{8}$$

as  $\delta \rightarrow 0$ . In addition, we illustrate with

$$f_{\text{sine}}(u) \equiv \sin(2\pi u) + a, \quad a \in [-1, 1] \tag{9}$$

and

$$f_{\text{cubic2}} \equiv \frac{1}{2}(u^2 - 3)u + a, \quad a \in [-1, 1]. \tag{10}$$

Returning to general smooth bistable nonlinearities  $f$  we have the following lemma.

**Lemma 2.1.** For  $f(u, \lambda) \in C^1$  satisfying (2) (with  $f'(u_{\pm})$  strictly positive),  $\lambda$  fixed, and  $u_- < u_0 < u_+$ , the travelling wave (4) connecting  $u_-$  and  $u_+$ , exists, is monotone and has finite wave speed.

**Proof.** Since  $f(u, \lambda) \in C^1$ , existence, monotonicity, and the fact that  $\varphi' \in L^2(\mathbb{R})$  follow from a straightforward geometric argument (see [11, 13]) and we have the necessary smoothness to multiply both sides of (4) by  $\varphi'$  and integrate with respect to  $\xi$ . One obtains

$$|c| = \left| \frac{\int_{u_-}^{u_+} f(v) \, dv}{\int_{\mathbb{R}} [\varphi'(\xi)]^2 \, d\xi} \right| \leq \frac{\max_{u \in [u_-, u_+]} |u_+ - u_-| |f(u, \lambda)|}{\int_{\mathbb{R}} [\varphi'(\xi)]^2 \, d\xi} < \infty. \quad \blacksquare$$

In [10], where  $f \equiv f_{\text{pwl}}$ , with  $u_- = 0, u_+ = 1$  and  $a \in [0, 1]$ , the wavespeed is

$$c = \frac{2\epsilon(2a - 1)}{\sqrt{1 - (2a - 1)^2}},$$

which is unbounded,  $\lim_{a \rightarrow 1^-} c(a) \rightarrow \infty$  and  $\lim_{a \rightarrow 0^+} c(a) \rightarrow -\infty$ . The function  $f_{\text{pwl}}$  is not  $C^1$  and  $f'(u_0)$  is not defined.

**Remark.** Using a geometric argument it is straightforward to show that if  $\lambda$  can be fixed such that  $u_0 = u_-$  ( $u_0 = u_+$ ), then there exists a  $c_-^* < 0$  ( $c_+^* > 0$ ), associated with this  $\lambda$ , such that travelling wave solutions exist connecting  $\varphi(-\infty) = u_-$  to  $\varphi(\infty) = u_+$  for all  $c \leq c_-^* < 0$  ( $c \geq c_+^* > 0$ ) and no travelling wave solutions exist for  $0 > c > c_-^*$  ( $0 < c < c_+^*$ ).

**Remark.** Finding  $c_+^*$  and  $c_-^*$  is often of interest.

Suppose for some value of  $\lambda$  the root  $u_0 = u_-$  ( $u_0 = u_+$ ), call it  $\lambda^*$ , and suppose  $\lim_{\lambda \rightarrow \lambda^*} u_0(\lambda) = u_0(\lambda^*) = u_-$  ( $\lim_{\lambda \rightarrow \lambda^*} u_0(\lambda) = u_0(\lambda^*) = u_+$ ), then  $\lim_{\lambda \rightarrow \lambda^*} c(\lambda) = c_-^*$  ( $\lim_{\lambda \rightarrow \lambda^*} c(\lambda) = c_+^*$ ).

This is illustrated in figure 1 when the nonlinearity is  $f_{\text{cubic}}$ .

### 3. Discretizations and travelling waves

We now present the temporal, spatial and complete discretizations and the resulting travelling wave equations. The temporal discretizations of the Nagumo PDE that we consider here are  $A(\alpha)$  stable linear multistep methods and the spatial discretizations are uniform finite differences. After defining the discretizations, we summarize our theoretical results to follow and outline a numerical technique that we employ to illustrate some of these results.

#### 3.1. Linear multistep methods and travelling wave solutions

We consider the effect of discretization on travelling solutions by applying a time discretization scheme to the PDE (1), applying the appropriate travelling wave ansatz, and then analysing the resulting travelling wave equations. Consider the application of a consistent implicit linear multistep method (see [15]) to the differential equation  $\dot{u} = g(u)$ . The resulting difference equation has the form  $\sum_{j=0}^k \alpha_j U_{n+j} = \Delta t \sum_{j=0}^k \beta_j g(U_{n+j})$  where  $U_{n+j} \approx u(t_{n+j})$  with  $\beta_k \neq 0$ . For (1) we obtain

$$\sum_{j=0}^k \alpha_j U_{n+j}(x) = \Delta t \sum_{j=0}^k \beta_j [\epsilon^2 \Delta U_{n+j}(x) - f(U_{n+j}(x))]. \quad (11)$$

The travelling wave ansatz becomes  $\Psi(x \cdot \sigma - ct_k) = U_k(x)$ , which upon substitution into (11) yields the travelling wave equations

$$\sum_{j=0}^k \alpha_j \Psi(\xi - jc\Delta t) = \Delta t \sum_{j=0}^k \beta_j [\epsilon^2 \Psi(\xi - jc\Delta t) - f(\Psi(\xi - jc\Delta t))], \quad \begin{array}{l} \Psi(-\infty) = u_-, \\ \Psi(+\infty) = u_+. \end{array} \quad (12)$$

In particular, we will focus on  $k$ -step BDF methods, where for  $\dot{u} = g(u)$  we have

$$\sum_{j=1}^k \frac{1}{j} \partial^j U_{n+k} = \Delta t g(U_{n+k}) \quad \text{where } \partial U_n = U_n - U_{n-1}, \quad \partial^j U_n = \partial[\partial^{j-1} U_n].$$

**Remark.** The one-stage BDF method is the backward Euler method, and the two-stage ( $k = 2$ ) BDF method has  $\alpha_2 = 1$ ,  $\alpha_1 = -\frac{4}{3}$ ,  $\alpha_0 = \frac{1}{3}$ ,  $\beta_2 = \frac{2}{3}$  and  $\beta_1 = \beta_0 = 0$ . The  $k$ -step BDF methods are  $A(\alpha)$  stable for  $k = 1, \dots, 6$ .

In section 4 we show that the behaviour of monotone travelling wave solutions to the stable BDF temporal discretizations with sufficiently smooth bistable nonlinearity  $f$  can be

divided into three cases that are separated by two bifurcation values in  $\Delta t$ . Let  $\mu_k = \alpha_k/\beta_k$  for the  $k$ -step BDF method, let  $0 < \Delta t_2(\mu_k) \leq \Delta t_1(\mu_k)$ , and let the solution profile  $\Psi(\eta)$  be sufficiently smooth. (1) When  $\Delta t$  is sufficiently large,  $\Delta t > \Delta t_1(\mu_k)$  and the wave speed  $|c|$  increases to infinity for  $u_0 \in (u_-, u_+)$  bounded away from  $u_-$  and  $u_+$ , very different behaviour compared to the travelling waves of (5) whose wave speed is often bounded for  $u_0 \in [u_-, u_+]$  ( $|c|$  is bounded when  $|f'| < \infty$ ). (2) When  $\Delta t$  is sufficiently small,  $0 < \Delta t < \Delta t_2(\mu_k)$ , the  $a(c)$  curve and the solution profile are a perturbation of that for (5). (3) When  $\Delta t$  is in between the small and large cases,  $\Delta t_2(\mu_k) \leq \Delta t \leq \Delta t_1(\mu_k)$  ( $\Delta t_1$  may actually equal  $\Delta t_2$  making this case nonexistent), the  $a(c)$  behaviour is like that of the  $\Delta t$  small case and the solution profiles are like that of the  $\Delta t$  large case.

### 3.2. Spatial discretization and travelling waves

We now consider the spatial discretization of (1) with mesh widths of  $\Delta x_i, i = 1, \dots, n$ , in the coordinate directions, thus obtaining a spatially discrete equation of the form

$$u_i(x, t) = \epsilon^2 Lu(x, t) - f(u(x, t)),$$

$$Lu(x, t) = \sum_{i=1}^n \left\{ \frac{1}{\Delta x_i^2} [u(x + \Delta x_i e_i, t) + u(x - \Delta x_i e_i, t) - 2u(x, t)] \right\}, \quad (13)$$

where  $e_i$  is the  $i$ th unit vector. For (13) the travelling wave equations are  $(\varphi(x \cdot \sigma - ct) = u(x, t))$

$$-c\dot{\varphi}(\xi) = \epsilon^2 L_T \varphi(\xi) - f(\varphi(\xi)), \quad \xi = x \cdot \sigma - ct \in \mathbb{R},$$

$$L_T \varphi(\xi) = \sum_{i=1}^n \left\{ \frac{1}{\Delta x_i^2} [\varphi(\xi + \Delta x_i \sigma_i) + \varphi(\xi - \Delta x_i \sigma_i) - 2\varphi(\xi)] \right\} \quad (14)$$

together with the boundary conditions  $\varphi(-\infty) = u_-$  and  $\varphi(+\infty) = u_+$ .

As opposed to the travelling wave equations for the PDE (4), the travelling wave equations for the spatial discretization (14) depend on the spatial dimension  $n$  and direction of propagation  $\sigma$ . This is simply due to the fact that the Laplacian is isotropic (direction independent) while the finite difference operator is anisotropic [5–7]. In addition, as we will see, another major difference [19,20,24,34] between the behaviour of travelling wave solutions for PDE and the spatially discretized equation is that centred differencing slows down the speed of the travelling wave and creates the existence of stationary travelling wave profiles ( $c = 0$ ) when  $\int_{u_-}^{u_+} f(u) du \neq 0$ . When  $f$  is the cubic nonlinearity (3) this translates to an interval of  $a$  values about  $\frac{1}{2}$  for which the wave speed  $c = 0$ .

### 3.3. Complete discretization—backward Euler and rectangular spatial mesh

If we consider a backward Euler discretization in time and standard second-order finite differences in space, then the travelling wave equation for the complete discretization is

$$-\Psi(\xi) + \Psi(\xi - c\Delta t) = \Delta t [\epsilon^2 L_T \Psi(\xi - c\Delta t) - f(\Psi(\xi - c\Delta t))], \quad (15)$$

where  $L_T$  is given in (14). Rewriting (15) as the operator equation

$$H(\Psi, c, \lambda, \Delta t) = 0,$$

one typically specifies  $\Delta t$  and  $\lambda$  (or  $c$ ) and solves for  $(c, \Psi)$  (or  $(\lambda, \Psi)$ ). As we will see, when a solution exists for (15), the solution pair  $(c, \Psi)$  (or  $(\lambda, \Psi)$ ) is not necessarily unique. However, specifying  $\Delta t, \lambda$  and  $c$  will produce a unique  $\Psi(\xi)$  when a solution exists.

### 3.4. The behaviour of $\lambda$ as $|c|$ approaches 0 and $\infty$

When solving the travelling wave equation (4) of (1) and the travelling wave equations (12), (14) and (15) of the discretizations of (1), there are two parameters,  $c$  and  $\lambda$ . We can either fix  $c$  or  $\lambda$  and solve for the other. We choose to give the wave speed  $c$ . In addition, to clarify dependences, we let  $u_0(\lambda) = \lambda$ . For  $f_{\text{cubic}}$ , (3), the functions  $u_0(\lambda(c)) = \lambda(c) = a(c)$  for (4) are monotone and have a range  $[0, 1]$ . With the boundary conditions  $\varphi(-\infty) = \Psi(-\infty) = u_-$  and  $\varphi(+\infty) = \Psi(+\infty) = u_+$  we will investigate the  $u_0(c)$  curves for each of our discretized examples and, in particular, we examine the error in  $u_0$  ( $\text{Err}_{u_0}$  being the difference in  $u_0$  values of (4) and its discretizations to obtain the same wave speed  $c$ ) with particular attention to the cases  $|c| \rightarrow \infty$  and  $|c| \rightarrow 0$ . As we will see, when (4) is solved through discretization, as  $|c| \rightarrow \infty$ , the second derivative and second-order difference terms, the terms that come from the diffusion operator, go to zero. Thus, any differences in  $u_0$ , or the solution curves, come from the temporal discretization. As  $|c| \rightarrow 0$ , the first derivative and the first-order difference terms, the terms that come from the time derivative, go to zero. Thus, any differences in  $u_0$ , or the solution curves, come from the spatial discretization.

### 3.5. Numerical technique

In the sections following this one we include plots of the solution profiles and the  $\lambda(c) = u_0(c)$  relations. All four of our travelling wave equations (4), (12), (14) and (15), with  $f$  a cubic-like smooth nonlinearity satisfying (2), can be written as

$$G(\bar{v}, \mu) = 0, \quad (16)$$

where  $\bar{v} = \{v(x), \dots, v(x - kc\Delta t), v(x + \Delta x_1\sigma_1), \dots, v(x + \Delta x_1\sigma_1 - kc\Delta t), \dots, v(x - \Delta x_n\sigma_n - kc\Delta t)\}$  with boundary conditions  $v(-\infty) = 0$ ,  $v(\infty) = 1$ . For all but (15), equation (16) is a two-point boundary interval problem on an infinite interval that is transitionally invariant. Since (16) is nonlinear, and we are solving for both  $v$  and  $\mu$ , we linearize (16) by considering the variation with respect to  $v$  and  $\mu$  obtaining

$$G_{\bar{v}}(\bar{v}, \mu)\bar{w} + G_{\mu}(\bar{v}, \mu)b = 0,$$

which has the isolated solution  $w = d\bar{v}$  and  $b = \dot{\mu} = 0$  for any  $d \in \mathbb{R}$ . Thus, we add to (16) the condition  $\dot{\mu} = 0$ . When solving (15), we add a  $\varepsilon\bar{v}$  term to make it a two-point boundary interval problem and take  $\varepsilon \rightarrow 0\pm$ . We used an experimental collocation based boundary value problem solver for functional differential equations of mixed type, COLMTFDE [1], using appropriate boundary functions defined in terms of eigenfunctions of the linearization about  $u_-$  and  $u_+$  to truncate the infinite interval. Results were obtained by computing in double precision, compiled with True64 Fortran, and run on a Compaq/DEC Alpha chip.

## 4. Temporal discretization and travelling waves

When  $|c| \rightarrow 0$ , (12) has no time dependence and hence there is no difference in  $u_0$  or  $\Psi$  for (4) and (12) since the discretization methods considered here are the so-called regular time discretization methods (see [30]) that neither create nor destroy equilibrium solutions.

Applying linear multistep methods (in particular, we consider the BDF methods) to (4) we now explore the behaviour of  $u_0(c) = \lambda(c)$  and  $\varphi$  for  $c \neq 0$  and, in particular, for  $|c| \rightarrow \infty$ . Recall that for the undiscretized equations with (2),  $c$  is bounded for  $u_0 \in (u_-, u_+)$  (lemma 2.1). For the temporal discretized equation this is no longer necessarily true; we will see that the behaviour of  $u_0$  varies greatly depending on the size of  $\Delta t$ . When  $\Delta t$  is small, the solution

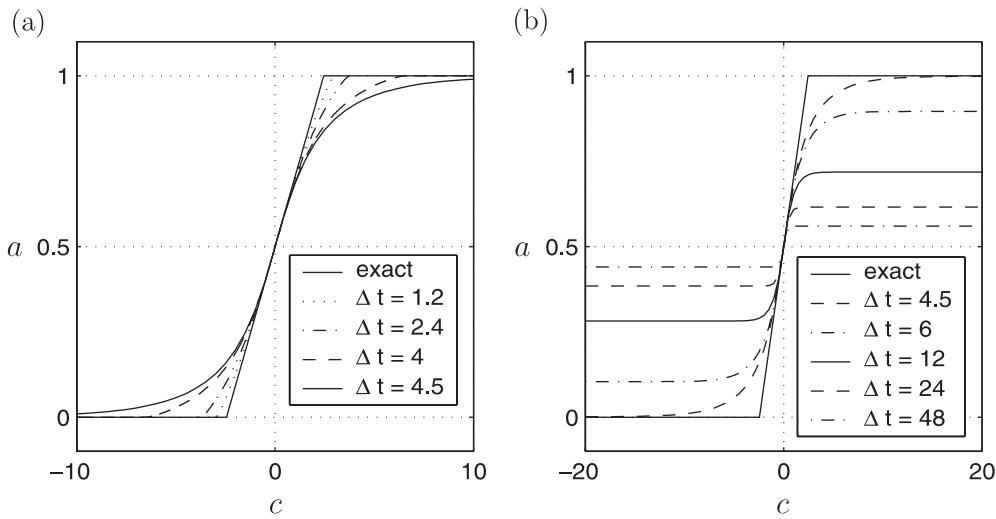


**Figure 2.** Two sets of  $a(c)$  curves generated by numerically solving the backward Euler version of (12), continuing in  $c$ , for various values of  $\Delta t$ , where in plot (a)  $\Delta t \in [0, 4]$  and in plot (b)  $\Delta t \in [9/2, \infty)$ .

and  $u_0(c)$  relation are a perturbation of the exact equation (4), for  $u_0 \in (u_-, u_+)$   $|c| < \infty$ . For instance, with the cubic nonlinearity,  $f_{\text{cubic}}$  (3), a perturbation of the solution (5), when  $\Delta t$  is large, we have behaviour much like that in the case of piecewise linear  $f_{\text{pwl}}(8)$  with backward Euler discretization [10], including the phenomenon of  $|c| \rightarrow \infty$  for values of  $u_0 \in (u_-, u_+)$ . The overall effect of applying these discretization methods to the travelling waves of (1) is wave speed-up, i.e. the speed of the travelling wave solution to the time discretized problem is larger than the speed of the travelling wave solution to the original problem for the same potential energy. Figure 2 illustrates wave speed-up.

Travelling wave solutions to (1), for a given bistable nonlinearity  $f$ , are monotone increasing (or decreasing) functions. The width of these travelling wave solutions (the ‘interface thickness’) is a function of the diffusion coefficient  $\epsilon$ ,  $c$  or  $\lambda$ , and of the nonlinearity  $f$ . For the BDF discretized equation, the interface thickness also depends on  $\Delta t$ . Let  $d(\epsilon, \text{tol})$  be the width of the interface for the discretized equation, where  $\text{tol} > 0$  is a small number (relative to  $u_+ - u_-$ ). Then, we define  $d$  to be the length of the interval in the independent variable  $d = |x_2 - x_1|$ , where  $x_1$  satisfies  $\Psi(x_1) - u_- = \text{tol}$  and  $x_2$  satisfies  $u_+ - \Psi(x_2) = \text{tol}$ .

**Remark.** While the following analysis focuses on the case when  $|c| \rightarrow \infty$ , with a straightforward perturbation argument, it also applies when  $|c| > d/\Delta t$  with the corrections due to the perturbation being of exponential size (i.e.  $e^{-|c|\Delta t}$ ).

For each of the temporal discretizations presented in this section, we consider the following formulation for large wavespeeds  $c$ . Assume  $c \neq 0$  and  $\Delta t > 0$ . Let  $\phi(\eta) = \Psi(\xi)$  with  $\eta = \xi/c$ . Then, the travelling wave equations for linear multistep methods, (12), become

$$\sum_{j=0}^k \alpha_j \phi(\eta - j\Delta t) = \Delta t \sum_{j=0}^k \beta_j \left[ \frac{\epsilon^2}{c^2} \ddot{\phi}(\eta - j\Delta t) - f(\phi(\eta - j\Delta t), \lambda) \right]. \tag{17}$$

Let  $\phi_{\pm}^*(\eta)$  be defined as  $\phi(\eta, c) \rightarrow \phi_{\pm}^*(\eta)$  as  $c \rightarrow \pm\infty$ . For  $|\ddot{\phi}(\eta)| < \infty, \eta \in \mathbb{R}$ , when  $c \rightarrow \pm\infty, \epsilon^2 \Delta t / c^2 \rightarrow 0$  and (12) can be written as the delay equation

$$\sum_{j=0}^k \alpha_{k-j} \phi_{\pm}^*(\eta + j \Delta t) = -\Delta t \sum_{j=0}^k \beta_{k-j} f(\phi_{\pm}^*(\eta + j \Delta t), \lambda), \tag{18}$$

where we have shifted the independent variable by  $k\Delta t$  (which does not affect the problem since the equation has translational invariance for shifts of length  $\Delta t$ ). Observe that for finite  $\eta$ ,

$$\phi_{\pm}^*(\eta + \Delta t) = \lim_{c \rightarrow \pm\infty} \phi(\eta + \Delta t) = \lim_{c \rightarrow \pm\infty} \Psi(\xi + c \Delta t) = u_{\pm}.$$

This is formalized in the following lemma.

**Lemma 4.1.** *Suppose  $\mu_k > 0$  and  $\phi_+^*(\eta_0) > u_0$  ( $\phi_-^*(\eta_0) < u_0$ ) for some  $\eta_0 \in \mathbb{R}$ . Then,  $\phi_+^*(\eta) = u_+$  ( $\phi_-^*(\eta) = u_-$ ) for all  $\eta \geq \eta_0$ .*

**Proof.** With  $\mu_k > 0$  we may assume  $\alpha_k$  and  $\beta_k > 0$ . Then, the right-hand side of (18) is non-negative (nonpositive) and the left-hand side is nonpositive (non-negative) for any smooth bistable nonlinearity  $f$ . The left- and right-hand sides are equal when  $\phi_+^*(\eta_0) = u_+$  ( $\phi_-^*(\eta_0) = u_-$ ) and the conclusion follows for monotone nondecreasing (nonincreasing) solutions. ■

For the  $k$ -step BDF methods (17)

$$\sum_{j=0}^k \alpha_j \phi(\eta - j \Delta t) = \Delta t \beta_k \left[ \frac{\epsilon^2}{c^2} \ddot{\phi}(\eta - k \Delta t) - f(\phi(\eta - k \Delta t), \lambda) \right]$$

and (18) is

$$\sum_{j=0}^k \alpha_{k-j} \phi_{\pm}^*(\eta + j \Delta t) = -\Delta t \beta_k f(\phi_{\pm}^*(\eta), \lambda). \tag{19}$$

Let  $\mu_k = \alpha_k / \beta_k$ . For the first six  $k$ -step BDF methods  $\mu_1 = 1, \mu_2 = 3/2, \mu_3 = 11/6, \mu_4 = 25/12, \mu_5 = 137/60$  and  $\mu_6 = 147/60$ .

4.1. General bistable nonlinearities

Consider a BDF temporal discretization of (1) and the resulting travelling wave equation (17) with general bistable nonlinearity. We discuss the case when  $c > 0, c < 0$  being similar. Define

$$\phi_c(\lambda) \in [u_-(\lambda), u_+(\lambda)] \quad \text{such that} \quad \frac{\partial f(\phi_c)}{\partial \phi} + \frac{f(\phi_c)}{u_+ - \phi_c} = 0.$$

Consider  $\Delta t$  large enough so that

$$\Delta t > \Delta t_1(\lambda) \equiv \frac{\mu_k(u_+ - \phi_c)}{f(\phi_c)} \quad \text{(Condition C1)} \tag{20}$$

We begin by considering equations (17) and (18) for the first six BDF methods, i.e.  $k = 1, \dots, 6$ , and  $\beta_0 = \dots = \beta_{k-1} = 0$ , and for  $\lambda = u_0$ , lemma 4.1 states that if  $\phi_+^* > u_0 = \lambda$  then  $\phi_+^* = u_+$ .

Now, suppose  $\phi_+^*(\eta_1) < u_0$  and  $\phi_+^*(\eta_1 + \Delta t) > u_0$ , for some  $\eta_1 \in \mathbb{R}$ , then, (19) is

$$g(\phi_+^*, u_0) \equiv f(\phi_+^*, u_0) + \frac{\mu_k}{\Delta t} (\phi_+^* - u_+) = 0 \tag{21}$$

(since  $\sum \alpha_j = 0$ ), which has the three real roots  $\phi_1(u_0, \Delta t)$ ,  $\phi_2(u_0, \Delta t)$  and  $\phi_3(u_0, \Delta t) = u_+$  when C1 (20) is satisfied. If we consider equation (17) for  $c$  large and positive, for the equation

$$\frac{\epsilon^2}{c^2} \ddot{\phi} = g(\phi, u_0), \tag{22}$$

the roots  $\phi_1$  and  $\phi_3$  can be thought of as the ‘stable’ equilibria and the root  $\phi_2$  as the ‘unstable’ equilibrium. Consider  $c$  large enough so the interface thickness  $\epsilon/c$  is much less than the height of the step, the distance from  $\phi_1$  to  $\phi_3$  (this distance turns out to be always greater than  $u_+ - \phi_c$ , where  $u_+ - \phi_c > 0$  if  $f_\phi(u_0) < \infty$ ), and so  $\epsilon/c$  is much less than the width of the step,  $\Delta t$ . We obtain boundary conditions by observing that as  $c \rightarrow \infty$ ,

$$\phi\left(\pm \frac{\Delta t}{2}\right) = \Psi\left(\pm \frac{c\Delta t}{2}\right) \rightarrow \Psi(\pm\infty) \quad \text{and} \quad \dot{\phi}\left(\pm \frac{\Delta t}{2}\right) = \dot{\Psi}\left(\pm \frac{c\Delta t}{2}\right) \rightarrow \dot{\Psi}(\pm\infty) = 0. \tag{23}$$

As  $|c| \rightarrow \infty$  the profile  $\Psi(\xi)$  has steps of infinite length. Thus,  $\phi(\pm\Delta t/2)$  will go to the values of  $\phi_+^*$  immediately above,  $\phi_3 = u_+$ , and below,  $\phi_1$ , the value of  $\Psi(0) = \phi(0)$  as  $c \rightarrow \infty$ . Suppose we want to find heteroclinic orbits connecting the ‘stable’ equilibria  $\phi_1$  and  $\phi_3$ , i.e. monotone solutions from  $\phi(-\Delta t/2) = \phi_1$  to  $\phi(\Delta t/2) = \phi_3$ , for a given  $\Delta t$  we wish to find  $u_0 = \lim_{c \rightarrow \infty} u_0(c)$ . Multiplying both sides of (22) by  $\dot{\phi}$ , integrating over  $\eta$  from  $-\Delta t/2$  to  $\Delta t/2$ , and setting the result equal to 0 gives

$$0 = \int_{\phi_1}^{\phi_3} g(\phi, u_0) d\phi = \int_{\phi_1}^{\phi_3} f(\phi, u_0) d\phi - \frac{\mu_k}{2\Delta t} [u_+ - \phi_1(u_0, \Delta t)]^2 \quad \text{(Condition C2)} \tag{24}$$

as a condition on  $u_0$ . This condition must be satisfied for a heteroclinic orbit from  $\phi_1$  to  $\phi_3$  to exist. Without this condition the real values  $\phi_1, \phi_2$  and  $\phi_3$  are just values of  $\phi$  where  $\ddot{\phi} = 0$ . As  $\Delta t \rightarrow \infty$ ,  $\phi_1 \rightarrow u_-$ , and since  $\phi_3 \rightarrow u_+$ , (24) defines the value of  $u_0$  such that  $\int_{u_-}^{u_+} f d\phi = 0$ . Because  $g$  is a continuous function of both  $u_0$  and  $\Delta t$ , for a  $u_0 \in (u_-, u_+)$ , there exists a value  $\Delta t_2(u_0) \geq \Delta t_1(u_0)$  such that C2 is satisfied.

The behaviour of the solutions to the stable backward differentiation formula temporal derivative approximations with a sufficiently smooth bistable nonlinearity  $f$  can be divided into three cases for  $u_0 \in (u_-, u_+)$ ,

- Case 1:  $\Delta t$  such that both conditions C1 and C2 are satisfied ( $\Delta t$  large),
- Case 2:  $\Delta t$  such that neither condition is satisfied ( $\Delta t$  small) and
- Case 3:  $\Delta t$  such that condition C1 is satisfied but not C2.

4.2. Case 1:  $\Delta t$  satisfies C1 and C2,  $\Delta t$  large

In this case the wave speed  $|c|$  increases to infinity for  $u_0$  bounded away from, and in between,  $u_-$  and  $u_+$ . Conditions C1 and C2 together ( $\Delta t = \Delta t_2$ ) are sufficient conditions for the formation of an additional ‘stable’ value.

**Example 4.1.**  $f$  is  $f_{\text{cubic}}$ . For the cubic nonlinearity (3),  $u_- = 0, u_0 = a, u_+ = 1, \phi_c = a/2$  and  $\Delta t_1 = 4\mu_k/a^2$ ; thus, condition C1 (20) is  $4\mu_k < a^2\Delta t$ . This implies that the function

$$g(\phi_+^*, a) = (\phi_+^*)^3 - (a + 1)(\phi_+^*)^2 + \left(a + \frac{\mu_k}{\Delta t}\right)\phi_+^* - \frac{\mu_k}{\Delta t} = 0 \tag{25}$$

has three real roots, which are

$$\phi_1(a, \Delta t) = \frac{a - \sqrt{a^2 - 4\mu_k/\Delta t}}{2}, \quad \phi_2(a, \Delta t) = \frac{a + \sqrt{a^2 - 4\mu_k/\Delta t}}{2}, \quad \text{and} \quad \phi_3(a, \Delta t) = 1. \tag{26}$$

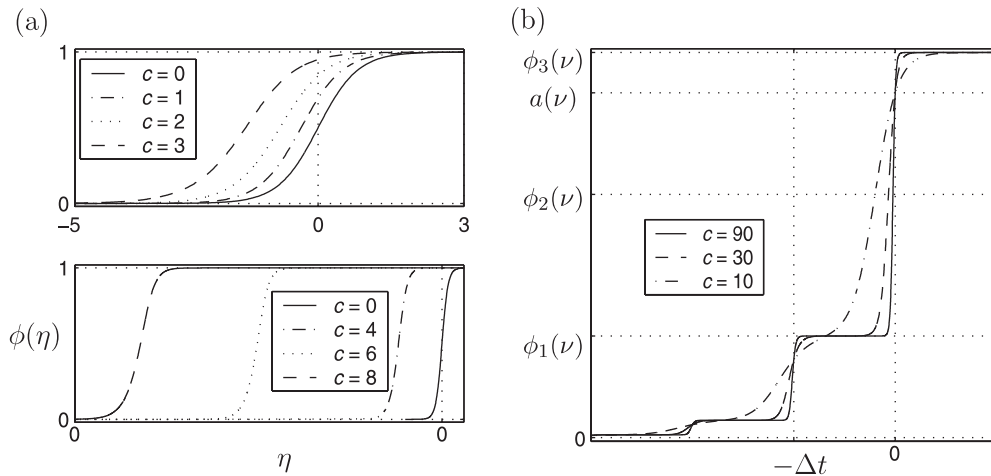


**Figure 3.** Plots for the backward Euler discretization with cubic nonlinearity for  $\epsilon^2 = 1$ . (a) The hyperbolic tangent shaped solution curves that are generated for  $\Delta t < 4$  and  $c$  large. (b) Three solution profiles found as described in section 3.5 for the large  $c$  values of 10, 30 and 90 when  $\Delta t = \nu \equiv 6$  ( $\Delta t$  large case). Here, we see that as  $c \rightarrow \infty$  the step width equals  $\Delta t$ . Note that when  $\Delta t = \nu$  the values obtained using (26) and (24),  $\phi_1(\nu) \approx 0.263\,762\,62$ ,  $\phi_2(\nu) \approx 0.631\,879\,72$ ,  $a(\nu) \approx 0.895\,643\,94$  and  $\phi_3(\nu) = 1$ , are exactly the same values of  $\phi$  at which  $\dot{\phi} = 0$ .

If we consider equation (17) for  $c$  large and positive, figure 3(b) demonstrates the validity of equation (22) and the boundary conditions (23) on  $\phi$  and  $\dot{\phi}$ . As in the  $f_{pwl}$  case (as shown in [10]), as  $|c| \rightarrow \infty$  the profile  $\Psi(\xi)$  has steps of infinite length. Thus,  $\phi(\pm\Delta t/2)$  will go to the values of  $\phi_+^*$  immediately above,  $\phi_3 = 1$ , and below,  $\phi_1$ , the value of  $\Psi(0) = \phi(0)$  as  $c \rightarrow \infty$ , as illustrated in figure 3(a).

Satisfying C2 defines heteroclinic orbits connecting the ‘stable’ equilibria  $\phi_1$  and  $\phi_3$ , i.e. defines monotone solutions from  $\phi(-\Delta t/2) = \phi_1$  to  $\phi(\Delta t/2) = \phi_3$ , for a given  $\Delta t$ . From this we wish to find  $a = \lim_{c \rightarrow \infty} a(c)$ . C2 is

$$0 = \int_{\phi_1}^{\phi_3} g(\phi, a) \, d\phi = \frac{1}{2} \left[ -\frac{a^4}{12} + \frac{a^3}{6} + \frac{a^2\mu_k}{2\Delta t} - \frac{a\mu_k}{\Delta t} - \frac{1\mu_k^2}{4(\Delta t)^2} \right] + \frac{1}{3} \left[ \frac{a^3}{8} - \frac{a^2}{4} - \frac{a\mu_k}{2\Delta t} + \frac{\mu_k}{\Delta t} \right] \sqrt{a^2 - \frac{4\mu_k}{\Delta t}} + \frac{1-2a}{12} + \frac{\mu_k}{2\Delta t} \tag{27}$$

and is plotted in figure 4.

Figure 4 illustrates both C1 and C2. The value of  $u_0 = a$  can be calculated directly from (27) and  $\Delta t_2(u_0) \in [9\mu_k/2, \infty)$ ,  $u_0 = a \in (0.5, 1]$  (figure 4), and the values  $\phi_1$  and  $\phi_2$  can be calculated using (26). This is the value of  $a$  that is obtained by solving (17) for fixed  $\Delta t$  following the continuation as  $c \rightarrow \infty$ . For comparison, numerically solving the backward Euler version (17) we obtain, for various  $c$ , the same values for  $a$ ,  $\phi_1$  and  $\phi_2$  that we calculated directly above, shown in figure 2(b). Figure 3(b) shows that the solutions are step-like and have three equilibrium points (two stable). This is very different from the solution to the exact (the undiscretized) equation, which behaves much like the travelling wave solutions to the Fisher equation as  $|c| \rightarrow \infty$ , with two of the roots of  $f_{cubic}$  sharing the same value.

The following theorem is a result of the fact that  $|c| \rightarrow \infty$  with  $u_0 \in (u_-, u_+)$ .

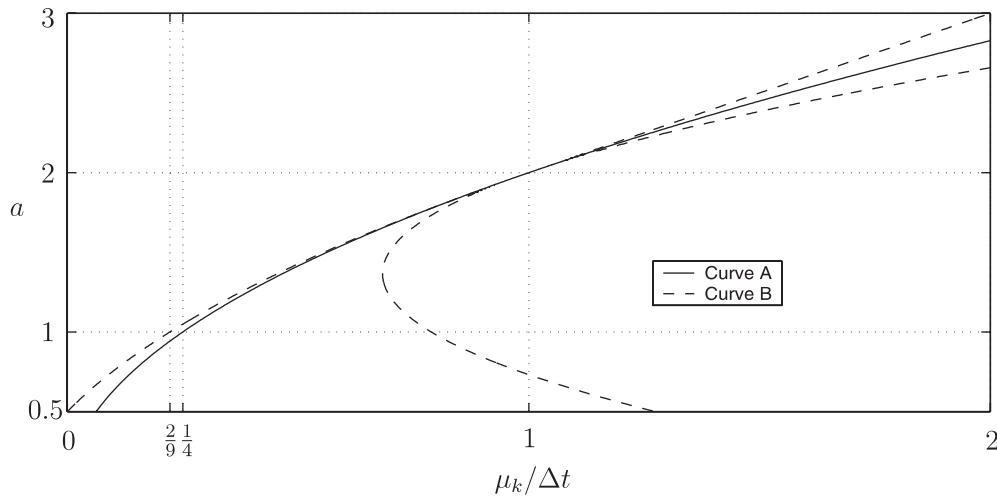


**Figure 4.**  $f = f_{\text{cubic}}$ . Curve A is a plot of the equation  $a^2 - 4\mu_k/\Delta t$  above which  $g(a, \Delta t)$ , defined in (25), has three real roots (C1). Curve B is a plot of (27), C2, the condition that gives us a heteroclinic orbit between  $\phi_1$  and  $\phi_3$ , where  $\phi_1$  and  $\phi_3$  are saddle points.

**Theorem 4.2.** For the travelling wave version of the  $k$ -step BDF discretization,  $k = 1, \dots, 6$ , of (1) with cubic nonlinearity (3), with  $\Delta t > \frac{9}{2}\mu_k$ ,

$$\lim_{|c| \rightarrow \infty} \text{Err}_a = \frac{5 - \sqrt{1 + 8(9\mu_k/\Delta t + 1)}}{4} \quad \text{and} \quad \lim_{c \rightarrow \pm\infty} a(c) = \frac{1}{2} \pm \frac{\sqrt{1 + 8(9\mu_k/\Delta t + 1)} - 3}{4}. \tag{28}$$

**Proof.** Since  $\Delta t > \frac{9}{2}\mu_k$  there is a  $u_0 = a \in (0, 1)$  that can be calculated from C2. By subtracting this  $a$  value (28) from 1 the  $\lim_{c \rightarrow \infty} \text{Err}_a$  follows. The case for  $c \rightarrow -\infty$  follows a similar analysis. ■

**Example 4.3.**  $f$  is  $f_{\text{sine}}$ . Consider the nonlinearity (9), where  $u_- = -(1/2\pi) \sin^{-1}(a)$ ,  $u_0 = 1/2 + (1/2\pi) \sin^{-1}(a)$ , and  $u_+ = 1 - (1/2\pi) \sin^{-1}(a)$ . Condition C1 is illustrated by curve A in figure 5, which defines the value of  $\Delta t_1$  with respect to  $a$  and  $\mu_k$ . Thus, for all values of  $a$  above curve A there exist three roots to  $g(\phi, a)$ . Because of the symmetric nature of this nonlinearity about  $\frac{1}{2}$ , condition C2 will only be satisfied when  $\phi_2 = \frac{1}{2}$ , when  $\phi_3 = u_+ = 1 - (1/2\pi) \sin^{-1}(a)$ , and when  $\phi_1 = 1 - \phi_3 = (1/2\pi) \sin^{-1}(a)$ . Thus, C2 is

$$\int_{\phi_1}^{1-\phi_1} g_{\text{sine}}(\phi, a) \, d\phi = -\frac{2\mu_k}{\Delta t} \phi_1^2 + \left(2a + \frac{2\mu_k}{\Delta t}\right) \phi_1 - \left(a + \frac{\mu_k}{2\Delta t}\right) = 0.$$

Solving for  $\phi_1$  we get

$$\phi_1 = \frac{1}{2} - a \frac{\Delta t}{\mu_k}.$$

Since  $\phi_1$  also equals  $\sin^{-1}(a)/(2\pi)$  we have

$$\frac{\mu_k}{\Delta t} = \frac{2\pi a}{\pi - \sin^{-1}(a)}, \tag{29}$$

which is curve B in figure 5.

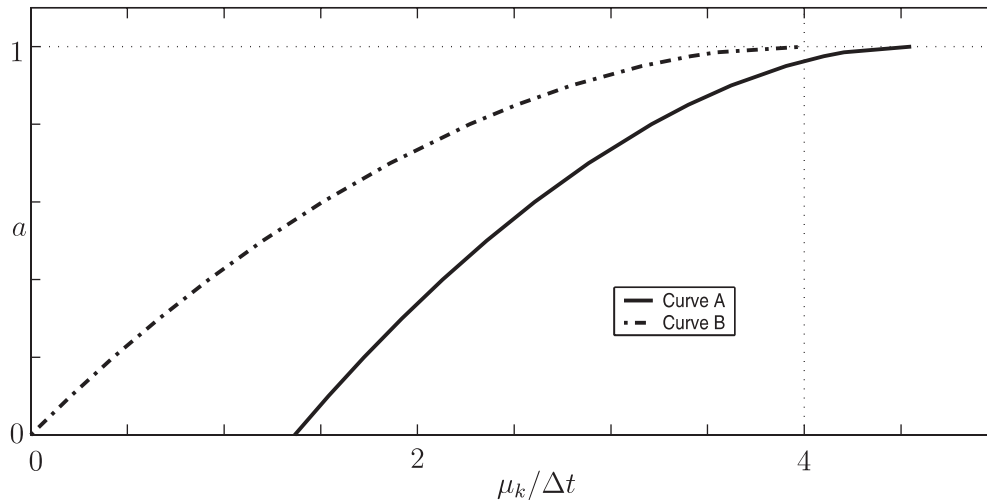


**Figure 5.**  $f = f_{\text{sine}}$ . Curve A is a plot of the equation above which  $g_{\text{sine}}(a, \Delta t)$ , has three real roots (C1). Curve B is a plot of (29), C2, the condition that gives us a heteroclinic orbit between  $\phi_1$  and  $\phi_3$ , where  $\phi_1$  and  $\phi_3$  are saddle points.

**Example 4.4.**  $f$  is  $f_2$ . In this example, the values of  $\phi_c$ ,  $\Delta t_1$ , etc can easily be calculated explicitly; however, their expressions are quite messy and, therefore, we only state bounding values to avoid unnecessary obfuscation of the presentation. When we consider the nonlinearity (7),  $u_- = 0$ ,  $u_+ = 1$  and  $\phi_c \in (a - \delta, a)$ , and because

$$f_2(\phi) \leq \frac{f_2(\phi_c)}{\phi_c - 1}(\phi - 1) \quad \text{for } \phi \leq 1,$$

condition C1 is satisfied for

$$\Delta t > \mu_k \frac{1 - a + \delta}{a - \delta} = \mu_k \frac{1 - a + \delta}{f_2(a - \delta)} \geq \mu_k \frac{1 - \phi_c}{f_2(\phi_c)} = \Delta t_1.$$

As  $\delta \rightarrow 0$ ,  $u_0 \rightarrow a$ ,  $\phi_c \rightarrow a$ , and condition C1, as well as the above estimate, become  $\Delta t > \mu_k(1 - a)/a = \Delta t_1$ . The root  $\phi_3 = 1$  and, for  $\delta$  small enough (or  $\Delta t$  large enough),  $\phi_1 = \mu_k/(\mu_k + \Delta t)$ . This implies that condition C1 is satisfied as long as  $\phi_1 < a = \phi_2$ . In other words, for any positive  $\Delta t$  there exists an  $a \in (0, 1)$  such that condition C1 is satisfied as long as  $\delta$  is small enough. Condition C2 is

$$\int_{\phi_1}^{\phi_3} f_2(\phi, u_0) \, d\phi - \frac{1}{2} \frac{\mu_k}{\mu_k + \Delta t} = 0.$$

As  $\delta \rightarrow 0$ ,

$$\int_{\phi_1}^{\phi_3} f_2(\phi, u_0) \, d\phi \rightarrow a - \frac{1}{2} - \frac{1}{2} \left( \frac{\mu_k}{\mu_k + \Delta t} \right)^2$$

and thus as  $\delta \rightarrow 0$ ,

$$\lim_{c \rightarrow \infty} u_0(c) = \lim_{c \rightarrow \infty} a(c) = \frac{1}{2} + \frac{\mu_k}{2(\mu_k + \Delta t)}$$

for all  $\Delta t > 0$ . Of course this turns out to be exactly the same result which is obtained for the piecewise continuous nonlinearity  $f_{\text{pwl in}}$  in [10] through direct construction.

4.3.  $\Delta t$  small ( $0 < \Delta t < \Delta t_1$ )

Again we focus on the  $c > 0$  case. Here, neither C1 nor C2 is satisfied. When  $\Delta t < \mu_k(u_+ - \phi_c)/f(\phi_c)$ ,  $g$  (21) has only one real root,  $u_+$ , when  $c$  is very large and hence the flow from  $u_+$  to  $u_-$  is not significantly modified when compared to the undiscretized travelling wave. We begin this case with a look at the  $\lambda(c)$  relation for  $\lambda = u_0 \in (u_-, u_+)$ . Although the following results are for  $\Delta t$  ‘sufficiently’ small, we will formally apply them for  $0 < \Delta t < \Delta t_1$ . We now show how to calculate  $\text{Err}_\lambda$  in terms of  $\Delta t$  to as much accuracy as desired for the  $k$ -step BDF methods.

Recall that the  $k$ -step BDF version of (12) can be written as

$$\sum_{j=0}^k \alpha_{k-j} \Psi(\xi + jc\Delta t) = \beta_k \Delta t [\epsilon^2 \ddot{\Psi}(\xi) - f(\Psi(\xi), \lambda)] \tag{30}$$

and assume that  $\Delta t$  is sufficiently small and  $\Psi(\xi)$  is sufficiently smooth so that we may expand

$$\Psi(\xi + jc\Delta t) = \Psi(\xi) + \dot{\Psi}(\xi)jc\Delta t + \dots = \sum_{n=0}^{\infty} \frac{\Psi^{(n)}(\xi)(jc\Delta t)^n}{n!}.$$

Approximating  $\Psi(\xi + jc\Delta t) \approx \sum_{n=0}^k (\Psi^{(n)}(\xi)(jc\Delta t)^n)/n!$  and substituting into (30), we obtain

$$-c\dot{\Psi}(\xi) = \epsilon^2 \ddot{\Psi}(\xi) - f(\Psi(\xi), \lambda),$$

the exact travelling wave equation (4), using theorem 3.5.3 from [30]. So, to order  $k$ , the  $k$ -step BDF methods have no difference in the  $\lambda$  values for the same wave speed  $c$ . In order to determine the  $\text{Err}_\lambda$  due to discretization we add the  $\Psi^{(k+1)}(\xi)(jc\Delta t)^{k+1}/(k+1)!$  term to the approximation of  $\Psi(\xi + jc\Delta t)$ , substitute, simplify and solve

$$-c\dot{\Psi}(\xi) = - \left[ \sum_{j=0}^k j^{k+1} \alpha_{k-j} \right] \frac{c^{k+1} \Delta t^k}{(k+1)!} \Psi^{(k+1)}(\xi) + \epsilon^2 \ddot{\Psi}(\xi) - f(\Psi(\xi), \lambda).$$

When  $k = 1$  this becomes a modification of the diffusion coefficient,

$$-c\dot{\Psi}(\xi) = \left( \frac{c^2 \Delta t}{2} + \epsilon^2 \right) \ddot{\Psi}(\xi) - f(\Psi(\xi), \lambda).$$

**Example 4.5.**  $f$  is  $f_{\text{cubic}}$ . For the cubic nonlinearity (3) with  $k = 1$  the  $u_0(c) = \lambda = a(c)$  relation is  $a = \frac{1}{2} + c/\sqrt{\Delta t c^2 + 2\epsilon^2}$ ,  $c \in (-\epsilon\sqrt{2}/\sqrt{4 - \Delta t}, \epsilon\sqrt{2}/\sqrt{4 - \Delta t})$ , and the error is

$$\text{Err}_a \approx \left| \frac{c}{\epsilon\sqrt{2}} - \frac{c}{\sqrt{\Delta t c^2 + 2\epsilon^2}} \right|, \quad \text{for } c \in \left[ -\frac{\epsilon}{\sqrt{2}}, \frac{\epsilon}{\sqrt{2}} \right],$$

$$\text{Err}_a \approx \left| \frac{1}{2} - \frac{c}{\sqrt{c^2 \Delta t + 2\epsilon^2}} \right|, \quad \text{for } c \in \left( -\frac{\epsilon\sqrt{2}}{\sqrt{4 - \Delta t}}, -\frac{\epsilon}{\sqrt{2}} \right) \cup \left( \frac{\epsilon}{\sqrt{2}}, \frac{\epsilon\sqrt{2}}{\sqrt{4 - \Delta t}} \right),$$

and for all other values of  $c$ , the value of  $a$  is either 0 or 1; see figure 2(a).

4.4.  $\Delta t$  such that  $\Delta t > \Delta t_1$  but does not satisfy C2 for  $u_0 \in [u_-, u_+]$

We discuss the case for  $c > 0$ , the case for  $c < 0$  being similar. As in the previous case, when restricting  $\lambda = u_0 \in [u_-, u_+]$ ,  $u_0 = u_+$  for some finite value of  $c$  and for all  $c$  larger. Let  $c$  be large. Let  $\Delta t > \mu_k(u_+ - \phi_c)/f(\phi_c)$  but not large enough, so that there exists a  $u_0 \in (u_-, u_+)$  that satisfies C2 (note: this case may not exist for all smooth bistable nonlinearities  $f$ ). The

function  $g(\phi_*, u_0)$ , (21), still has the three real roots (26) but no  $u_0 \in [u_-, u_+]$  satisfies (24); i.e. the integral  $\int_{\phi_1}^{\phi_3} g(\phi, u_0) \neq 0$ . Although  $\phi_1 < \phi_2 < \phi_3 = u_+$  are values of  $\phi$  where  $\ddot{\phi} = 0$ , there no longer exists a heteroclinic orbit between  $\phi_1$  and  $\phi_3 = u_+$  as in the case where  $\Delta t$  is large enough such that C2 was satisfied for some  $u_0 \in (u_-, u_+)$ . However, in the limit  $|c| \rightarrow \infty$ , we still have a solution that is a discrete set of values, only now they truly connect  $u_-$  and  $u_+$ , the same behaviour we are about to discuss in section 5 for the spatially discretized equation (14) for  $|c| \rightarrow 0$ .

When numerically solving this example the choice of phase condition is critical, it enforces the bound on  $u_0$  of  $[u_-, u_+]$ . For  $|c|$  large we obtained travelling wave solutions that are very much like the solutions to the Fisher equation for  $\Delta t$  small.

**Example 4.6.**  $f$  is  $f_{\text{cubic}}$ . As in the previous case, when restricting  $\lambda = u_0 \in [u_-, u_+]$ ,  $u_0 = u_+$  for some finite value of  $c$  and for all  $c$  larger. Let  $c$  be large and  $4\mu_k < \Delta t < 9\mu_k/2$ . The function  $g(\phi_*, 1)$ , defined in (25), still has the three real roots (26) but, as figure 4 shows, a no longer satisfies (24), i.e. the integral  $\int_{\phi_1}^{\phi_3} g(\phi, 1) \neq 0$ , but does satisfy the relation  $\phi_2 = 1 - \phi_1$ . Although  $\phi_1 < \phi_2 < \phi_3 = 1$  are values of  $\phi$  where  $\ddot{\phi} = 0$ , there no longer exists a heteroclinic orbit between  $\phi_1$  and  $\phi_3 = 1$  as in the  $\Delta t > 9\mu_k/2$  case. However, in the limit  $|c| \rightarrow \infty$ , we still have a solution that is a discrete set of values, only now they truly connect 0 and 1.

For  $|c|$  large we obtained travelling wave solutions that are very much like the solutions to the Fisher equation when  $\Delta t < 4\mu_k$ . If we do not restrict  $a$  to  $[0, 1]$ , however, there also exist stable travelling wave solutions and heteroclinic orbits between  $\phi_1$  and  $\phi_3 = 1$ , for  $4\mu_k < \Delta t < 9\mu_k/2$ , which are more stable than the solutions that we desire, they are connecting orbits between saddle points in the  $\Delta t > 9\mu_k/2$  case. Figure 4 shows the values of  $a$ , outside  $[0, 1]$ , for these solutions.

## 5. Uniform spatial discretization

In this section, we find the error in the parameter  $\lambda = u_0$  as a function of  $c$  and in the wave speed  $c$  as a function of  $\lambda$ , by examining the difference in the  $(\lambda, c)$  relationships for (4) and (14). We are primarily interested in the case when  $u_-(\lambda)$ ,  $u_0(\lambda) = \lambda$  and  $u_+(\lambda)$  are three distinct values ( $u_- < u_0 < u_+$ ), but we also discuss the case when  $u_0$  equals either  $u_-$  or  $u_+$ . When  $u_- < u_0 < u_+$  we expect the wave speed to be finite valued and the solution profiles and wave speed solutions to be unique. When we have a degenerate root of the nonlinearity, i.e. when  $u_0$  equals either  $u_-$  or  $u_+$ , the equations and their solutions behave like that of the Fisher equation, including the absence of an upper bound on the magnitude of the wave speed. In the infinite wave speed limit, the spatial derivatives and differences no longer affect the solution profile or the value of  $\lambda$ , and thus the error goes to zero. The error due to spatial discretization is most dramatic in the zero wave speed limit; not only is the error in the  $\lambda, c$  relationship not equal to zero, but the behaviour of the solution profile and the  $\lambda(c)$  relation are fundamentally different for (4) and (14), the solutions of (14) exhibiting propagation failure and step-like profiles, phenomena not present in the solutions of (4).

### 5.1. When $u_- < u_0 < u_+$

Assume  $f$  has the necessary smoothness. Let  $c$  be the wave speed and  $\varphi(\xi)$  be the solution of (4), and let  $c_{\Delta x}$  be the wave speed and  $\varphi_{\Delta x}(\xi)$  be the solution of the spatial discretized equation (14). The intent of this section is to demonstrate that, for a fixed value of  $u_0$  (or  $\lambda$ ),  $|c| \geq |c_{\Delta x}|$ . This section consists of two subsections, one where the minimum of the nonzero  $\Delta x_i$ ,  $\Delta x_{\min}$ , is large—large enough that (14) exhibits propagation failure—and one where the

maximum of the  $\Delta x_i$ ,  $\Delta x_{\max}$ , is small—small enough that a nonzero wave speed and a unique monotone solution exist. Both  $\Delta x_{\min}$  and  $\Delta x_{\max}$  depend on  $c$ ,  $\lambda$  and  $\epsilon$  and the two above cases may overlap. This can be seen in the fact that there are values of  $\lambda$  and  $\epsilon$  such that there is exponentially small resistance to motion for all nonzero  $\Delta x_{\min} \neq 0$ . The terms large and small are dependent on the strength of the nonlinearity and the size of the diffusion coefficient  $\epsilon^2$ .

5.1.1.  $\epsilon/\Delta x_{\max}$  is large. Here, we assume that  $\Delta x_{\max}$  is small enough that the existence, uniqueness and global stability results, [33, 34], for a travelling wave solution to (14) can be applied (this also assumes that  $\int_{-\infty}^{\infty} f(u, \lambda) du \neq 0$ ).

**Lemma 5.1.** *If  $\int_{-\infty}^{\infty} (3[\ddot{\varphi}(\xi)]^2 - [(c/\epsilon^2)\dot{\varphi}(\xi)]^2)e^{(c/\epsilon^2)\xi} d\xi \geq 0$ , then, for any choice of  $\epsilon^2 > 0$  and  $\lambda$  such that  $u_- < u_0 < u_+$ ,  $|c_{\Delta x}| \leq |c|$ .*

**Proof.** We begin by changing variables, letting  $\phi(v) = \varphi(\xi)$  and  $\psi(v) = \varphi_{\Delta x}(\xi)$ , where  $v = \xi/\gamma$  for  $\gamma \geq 1$ . Then, (4) can be written as

$$-c_\gamma \dot{\phi}(v) = \frac{\epsilon^2}{\gamma^2} \ddot{\phi}(v) - f(\phi(v)) \quad \text{with } c_\gamma = \frac{c}{\gamma}, \tag{31}$$

and (14) becomes

$$-c_\delta \dot{\psi}(v) = \frac{\epsilon^2}{\gamma^2} L_p \psi(v) - f(\psi(v)) \quad \text{with } c_\delta = \frac{c_{\Delta x}}{\gamma}, \tag{32}$$

$$L_p \psi(v) = \sum_{i=1}^n \left\{ \frac{1}{\delta_i^2} [\psi(v + \delta_i \sigma_i) + \psi(v - \delta_i \sigma_i) - 2\psi(v)] \right\}, \quad \text{and} \quad \delta_i = \frac{\Delta x_i}{\gamma},$$

for  $i = 1, \dots, n$ .

In [17] a variational principle is proved that applies to (31) and (32) allowing us to make the following comparison in wave speeds. Note that the results in [17] assume that the travelling waves are stable. The results in [3] may be applied to show stability. Let  $\psi(v) = v(v) + \delta^2 w(v)$  and  $c_\delta = c_0 + \delta^2 c_1 + O(\delta^4)$ , where  $\delta = \max_{i=1, \dots, n} \delta_i$ . Then, (32) becomes

$$0 = [c_0 + \delta^2 c_1 + O(\delta^4)] [\dot{v} + \delta^2 \dot{w}] + \frac{\epsilon^2}{\gamma^2} L_p [v + \delta^2 w] - f(v + \delta^2 w).$$

Expanding the terms  $v(v \pm \delta_i \sigma_i)$  and  $w(v \pm \delta_i \sigma_i)$  about  $v$  in a Taylor series, and expanding  $f(\psi)$  about  $v$  in a Taylor series, we obtain

$$0 = [c_0 + \delta^2 c_1 + O(\delta^4)] [\dot{v} + \delta^2 \dot{w}] + \frac{\epsilon^2}{\gamma^2} \left[ \ddot{v} + \delta^2 \ddot{w} + 2 \sum_{j=2}^{\infty} \sum_{i=2}^n \frac{\delta_i^{2(j-1)} \sigma_i^{2j}}{2j!} (v^{(2j)} + \delta^2 w^{(2j)}) \right]$$

$$- \sum_{j=0}^{\infty} (\delta^2 w)^j f^{(j)}(v).$$

Assuming  $\gamma$  is large enough so that  $\delta^2 \ll 1$ , we begin by solving the leading order equation

$$0 = \left[ c_0 \dot{v} + \frac{\epsilon^2}{\gamma^2} \ddot{v} - f(v) \right],$$

which is (31), and hence  $v(v) = \phi(v)$  and  $c_0 = c_\gamma$ . Continuing, since  $\gamma$  is such that  $\delta^2 \gg \delta^4$ , we next want to solve

$$M[w] \equiv c_\gamma \dot{w} + \frac{\epsilon^2}{\gamma^2} \ddot{w} - f_v(v)w = -c_1 \dot{\phi} - \frac{\epsilon^2}{\gamma^2} \sum_{i=1}^n \left( \frac{\delta_i}{\delta} \right)^2 \frac{\sigma_i^4}{12} \phi^{(iv)}, \tag{33}$$

where  $w(\pm\infty) = 0$ . Since  $M[\dot{\phi}] = 0$ , the left-hand side of (33) is a noninvertible linear operator. Thus, a solution to (33) exists if and only if the right-hand side of (33) is orthogonal to the null space of the adjoint of  $M$ ,

$$M^*[u] = -c_\gamma \dot{u} + \frac{\epsilon^2}{\gamma^2} \ddot{u} - f_v(v)u.$$

Using the solution  $e^{c_\gamma A v} \dot{\phi}(v)$  of  $M^*[u] = 0$ , where  $A = \gamma^2/\epsilon^2$ , we find  $c_1$  with the solvability condition

$$c_1 \int_{-\infty}^{\infty} \dot{\phi}(v) \dot{\phi}(v) e^{c_\gamma A v} dv = -\frac{\epsilon^2}{\gamma^2} \sum_{i=1}^n \left(\frac{\delta_i}{\delta}\right)^2 \frac{\sigma_i^4}{12} \int_{-\infty}^{\infty} \phi^{(iv)}(v) \dot{\phi}(v) e^{c_\gamma A v} dv,$$

or

$$c_1 = -\frac{c_\gamma}{24} \sum_{i=1}^n \left(\frac{\Delta x_i \sigma_i^2}{\Delta x_{\max}}\right)^2 \frac{\int_{-\infty}^{\infty} (3[\ddot{\phi}(v)]^2 - [c_\gamma A \dot{\phi}(v)]^2) e^{c_\gamma A v} dv}{\int_{-\infty}^{\infty} \dot{\phi}(v) \dot{\phi}(v) e^{c_\gamma A v} dv}.$$

Hence, the sign of  $c_1$  is the opposite of the sign of  $c_\gamma$  when  $\int_{-\infty}^{\infty} (3[\ddot{\phi}(v)]^2 - [c_\gamma A \dot{\phi}(v)]^2) e^{c_\gamma A v} dv = \gamma^3 \int_{-\infty}^{\infty} (3[\ddot{\phi}(\xi)]^2 - [(c/\epsilon^2)\dot{\phi}(\xi)]^2) e^{(c/\epsilon^2)\xi} d\xi > 0$ . Thus  $|c| = \gamma|c_\gamma| \geq |\gamma c_\delta| = |c_{\Delta x}|$ . ■

*5.1.2. Propagation failure,  $\epsilon^2/(\Delta x_{\min})^2$  small.* When  $\epsilon^2/(\Delta x_{\min})^2$  is small enough the solution to the spatially discrete bistable reaction–diffusion equation (14) allows for zero wave speed  $c_{\Delta x}$  (and nonunique solutions) even though  $\int_0^1 f(\varphi, \lambda) \neq 0$ . MacKay and Sepulchre [22] (in terms of (14)) show that the implicit function theorem can be used to show that the stationary solutions that occur when  $\epsilon = 0$  can continue to be stationary solutions for  $\epsilon^2$  small along with a procedure for estimating a somewhat loose bound for  $\epsilon^2$ ,  $\epsilon_0^2$ . They do this by finding a bound of the norm of the inverse of the linearization of (14). To illustrate, let  $\varphi_{\text{cr}+}$  be the value of  $\varphi$  closest to  $u_-$  ( $u_+$ ) such that  $u_- < \varphi_{\text{cr}-} < u_0$  ( $u_+ > \varphi_{\text{cr}+} > u_0$ ) and  $f_\varphi(\varphi_{\text{cr}-}) = 0$  ( $f_\varphi(\varphi_{\text{cr}+}) = 0$ ). Letting  $\kappa = \sum_{j=1}^n 1/(\Delta x_j)^2$ , for monotone solutions, propagation failure occurs for

$$0 \leq \epsilon^2 \leq \epsilon_0^2 \equiv \frac{1}{\kappa} \int_b^d |\inf f_x(x)| dx. \tag{34}$$

Either  $b = u_-$ ,  $d = \varphi_{\text{cr}-}$  or  $b = \varphi_{\text{cr}+}$ ,  $d = u_+$  since  $f$  is monotone on the intervals  $(\varphi_-, \varphi_{\text{cr}-})$  and  $(\varphi_{\text{cr}+}, \varphi_+)$ . We summarize in the following theorem.

**Theorem 5.1.** *For equation (14) with a smooth nonlinearity and the  $\sigma_i \Delta x_i$ ,  $i = 1, \dots, n$  rationally related, when  $0 \leq \epsilon^2 \leq \epsilon_0^2$  there exists an interval of values of  $u_0 = \lambda$ , let us call it  $J$ , for which  $c = 0$  (known as the interval of propagation failure).*

**Example 5.2.**  *$f$  is  $f_{\text{cubic}}$ . For the nonlinearity (3),  $\varphi(\varphi - a)(\varphi - 1)$ , the quantity  $\int_{-\infty}^{\infty} (3[\ddot{\phi}(\xi)]^2 - [(c/\epsilon^2)\dot{\phi}(\xi)]^2) e^{(c/\epsilon^2)\xi} d\xi > 0$  where  $(\varphi, c)$  is the solution of (4). Thus, for values of  $a$  such that  $c_{\Delta x} \neq 0$ ,  $|c_{\Delta x}| \leq |c|$ . Figure 6 illustrates that, in fact,  $c_{\Delta x}$  approaches  $c$  as  $\epsilon/\Delta x \rightarrow \infty$ .*

*The critical values for (3) are*

$$\varphi_{\text{cr}\pm} = \frac{a+1}{3} \pm \frac{\sqrt{a^2 - a + 1}}{3}$$

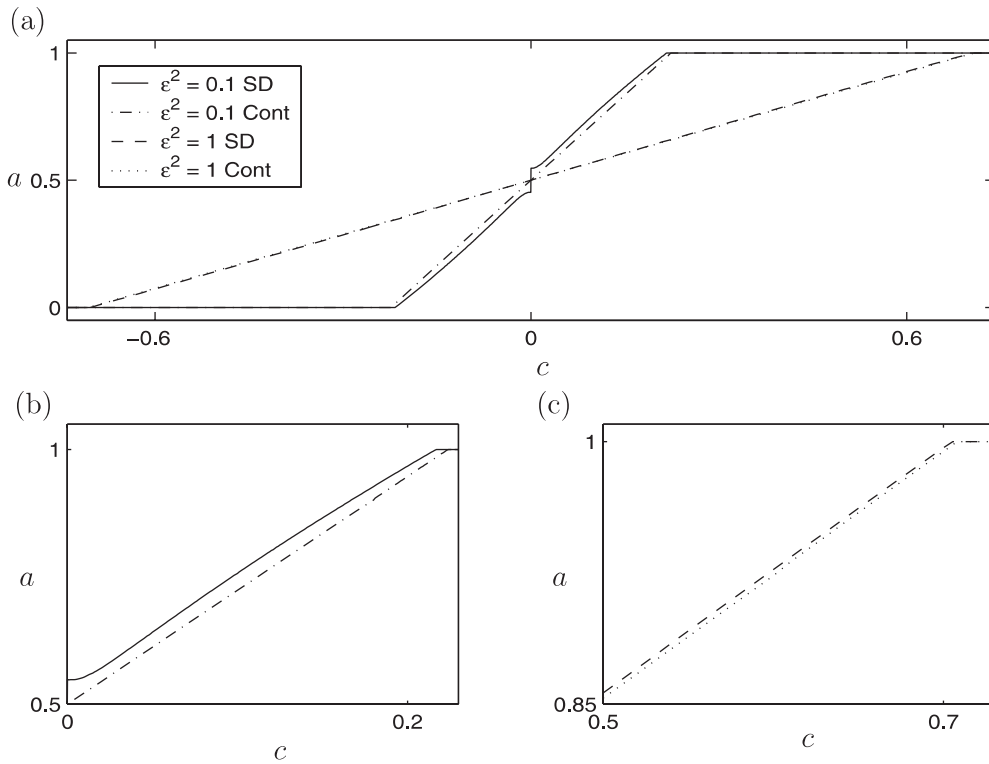


**Figure 6.** Plots of  $a(c)$  for the travelling wave formulations of both the spatial discrete (SD) equation (13) and the spatially continuous (Cont) equation (1) with the cubic nonlinearity  $f_2$ . To magnify propagation failure we let  $n = 1$ . For ease of calculation  $\Delta x_1 = 1$ . (a) The curves for the two values of  $\epsilon^2 = 0.1$  and 1. Here, we see that the error is much larger for the smaller value of  $\epsilon^2$ . (b) An enlargement of (a) for the  $\epsilon^2 = 0.1$  curves. Beside the larger error, this plot shows propagation failure. (c) An enlargement of (a) for the  $\epsilon^2 = 1$  curves.

and  $f$  is monotone on both the intervals  $[0, \varphi_{cr-}]$  and  $[\varphi_{cr+}, 1]$ . Thus, for

$$\epsilon^2 \leq \epsilon_0^2 \equiv \frac{1}{\kappa} \begin{cases} |f(\varphi_{cr+})| = \frac{2a^3 - 3a^2 - 3a + 2 + 2(a^2 - a + 1)^{3/2}}{27}, & a \geq \frac{1}{2}, \\ |f(\varphi_{cr-})| = \frac{2a^3 - 3a^2 - 3a + 2 - 2(a^2 - a + 1)^{3/2}}{27}, & a \leq \frac{1}{2}, \end{cases} \quad (35)$$

the wave speed  $c_{\Delta x} = 0$ .

Figure 7 illustrates  $h(a) \equiv \epsilon_0^2 \kappa$  versus  $a$  for the nonlinearity (3). Suppose  $\epsilon^2 \sum_{i=1}^n 1/\Delta x_i^2 = h(a) = 0.02$ . Then, the dashed line in figure 7 demonstrates that the interval  $[a_1, a_2]$  is included in the interval of propagation failure  $J$ .

The numerical studies found in [1, 7] show that for  $n = 1$  an interval of propagation failure exists for at least  $1/6 > \epsilon^2/\Delta x_1^2 \geq 0$ , a much larger interval of coefficient values than defined in theorem 5.1 above. Figure 6 shows an  $a(c)$  curve for  $n = 1$  and  $\epsilon^2/\Delta x_1^2 (= 1/10)$ , which admits an interval of propagation failure and an  $a(c)$  curve for  $n = 1$  and  $\epsilon^2/\Delta x_1^2 (= 1)$ , which appears to have no interval of propagation failure. However, the results of Fiedler and Scheurle [12] suggest the possibility of an exponentially small range of propagation failure that may not be resolved numerically.

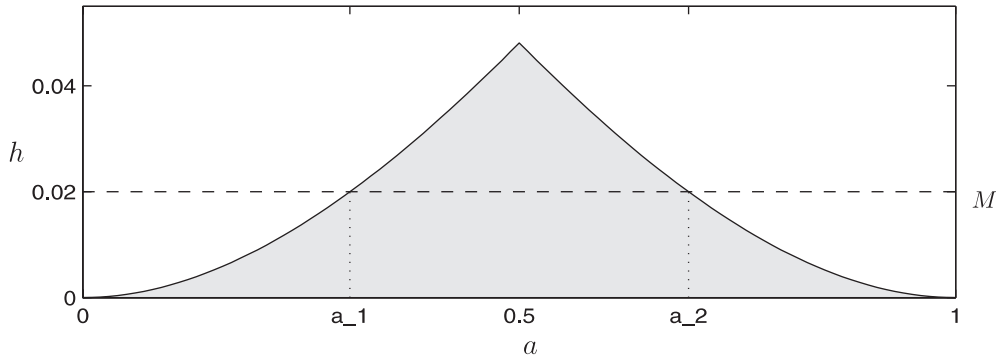


**Figure 7.** Plot of  $h(a)$ , defined in (35), is a tool for illustrating an interval of propagation failure and set valued  $a(c)$  functions.

**Example 5.3.**  $f$  is  $f_{\text{sine}}$  and  $f$  is  $f_{\text{cubic2}}$ . For the nonlinearity (9),  $\sin(2\pi\varphi) + a$ , and the nonlinearity (10),  $(\varphi^2 - 3)\varphi/2 + a$ , the quantity  $\int_{-\infty}^{\infty} (3[\tilde{\varphi}(\xi)]^2 - [(c/\epsilon^2)\tilde{\varphi}(\xi)]^2)e^{(c/\epsilon^2)\xi} d\xi > 0$ , where  $(\varphi, c)$  is the solution of (4). Thus, for values of  $a$  such that  $c_{\Delta x} \neq 0$ ,  $s |c_{\Delta x}| \leq |c|$ . Figure 6 illustrates that, in fact,  $c_{\Delta x}$  approaches  $c$  as  $\epsilon/\Delta x \rightarrow \infty$ .

The critical values for (9) and (10) are

$$\varphi_{\text{cr}\pm} = \frac{1}{2} \pm \frac{1}{4} \quad \text{and} \quad \varphi_{\text{cr}\pm} = \pm 1$$

respectively, and  $f$  is monotone on both the intervals  $[u_-, \varphi_{\text{cr}-}]$  and  $[\varphi_{\text{cr}+}, u_+]$  for both nonlinearities (recall  $u_- = -(1/2\pi) \sin^{-1}(a)$  and  $u_+ = 1 - (1/2\pi) \sin^{-1}(a)$ ). Thus, for both nonlinearities

$$\epsilon_{01}^2 \equiv \frac{1}{\kappa} \begin{cases} 1 - a, & a \geq 0, \\ 1 + a, & a \leq 0, \end{cases} \tag{36}$$

the wave speed  $c_{\Delta x} = 0$ .

Region II of figure 8 (where we have plotted  $h_1(a) \equiv \epsilon_{01}^2 \kappa$  versus  $(a + 1)/2$  for the nonlinearities (9) and (10)) illustrates the region of parameter space where theorem 5.1 guarantees propagation failure.

**Example 5.4.**  $f$  is  $f_1$  and  $f$  is  $f_2$ . The two nonlinearities in this example do not possess the necessary smoothness to apply lemma 5.1, but are smooth enough to apply theorem 5.1.

For the nonlinearity (7) the critical values are  $\varphi_{\text{cr}\pm} = a \pm \sqrt{\delta^2(1 - 4\delta/3)}$  and  $f$  is monotone on  $[0, \varphi_{\text{cr}-}]$  and  $[\varphi_{\text{cr}+}, 1]$ . As  $\delta \rightarrow 0$ ,  $\varphi_{\text{cr}\pm} \rightarrow a \pm$ . Thus,

$$\epsilon_{02}^2 \equiv \frac{1}{\kappa} \begin{cases} |f(\varphi_{\text{cr}+})| = -a + \frac{(9 - 12\delta)^{3/2}}{54} + \frac{1}{2}, & a \geq \frac{1}{2}, \\ |f(\varphi_{\text{cr}-})| = a + \frac{(9 - 12\delta)^{3/2}}{54} - \frac{1}{2}, & a \leq \frac{1}{2}. \end{cases} \tag{37}$$

Let  $h_2(a) = \epsilon_{02}^2 \kappa$ .

For the nonlinearity (6) the critical values are  $\varphi_{\text{cr}-} = a/(1 + \delta)$ ,  $\varphi_{\text{cr}+} = (a + \delta)/(1 + \delta)$  and  $f$  is monotone on  $[0, \varphi_{\text{cr}-}]$  and  $[\varphi_{\text{cr}+}, 1]$ . As  $\delta \rightarrow 0$ ,  $\varphi_{\text{cr}\pm} \rightarrow a \pm$ . Thus,

$$\epsilon_{03}^2 \equiv \frac{1}{\kappa} \begin{cases} |f(\varphi_{\text{cr}+})| = \frac{(1 - a)}{(1 + \delta)}, & a \geq \frac{1}{2}, \\ |f(\varphi_{\text{cr}-})| = \frac{a}{(1 + \delta)}, & a \leq \frac{1}{2}. \end{cases} \tag{38}$$

Let  $h_3(a) = \epsilon_{03}^2 \kappa$ .

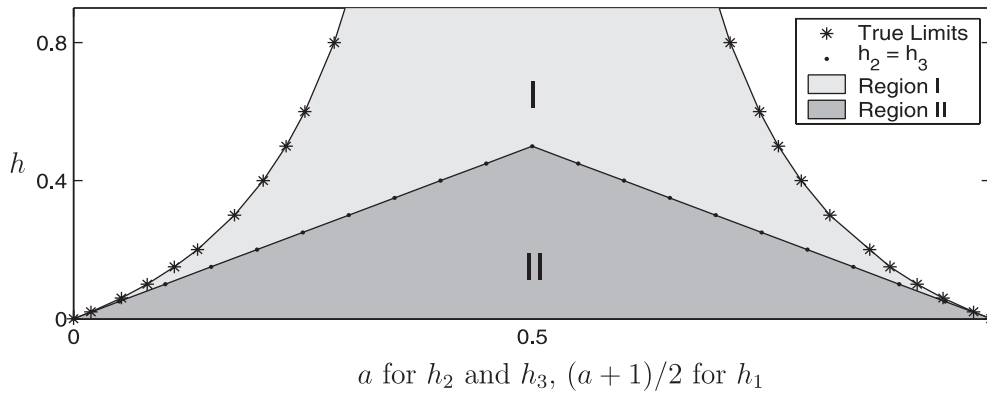


**Figure 8.** Plot of  $h(a)$  defined in (36)–(38), and is a tool for illustrating an interval of propagation failure and set valued  $a(c)$  functions.

For any given  $a \in [0, 1]$  both  $h_2$  and  $h_3$  obtain their maximum values when  $\delta \rightarrow 0$  and in fact  $\lim_{\delta \rightarrow 0} h_2(a, \delta) = \lim_{\delta \rightarrow 0} h_3(a, \delta)$  (the curves bounding Region II from above in figure 8). Thus, for  $\delta > 0$  the  $h_2(a)$  and  $h_3(a)$  values lie inside Region II. Region II illustrates the values of  $\epsilon^2 / \sum_{i=1}^n \Delta x_i$  and  $a$  for which a stationary monotone solution exists defined by theorem 5.1. The region of  $\epsilon^2 / \sum_{i=1}^n \Delta x_i$  and  $a$  where propagation actually exists in the  $\delta \rightarrow 0$  limit can be calculated using the techniques in [5] and Region I together with Region II, in figure 8, show the actual region of parameter space where a stationary monotone solution exists, thus illustrating that theorem 5.1 does not necessarily give a tight upper bound.

5.2. When  $a = u_0 = u_-$  or  $u_+$

The degenerate root in the nonlinearity allows a minimum (maximum) wave speed  $c_* > 0$  ( $c_* < 0$ ), such that for all  $|c| < |c_*|$  there does not exist a connecting orbit between  $u_-$  and  $u_+$  and for all  $|c| \geq |c_*|$  there does exist a connecting orbit. Recalling the solutions illustrated in figure 1 this is where stable heteroclinic solutions meet Fisher type solutions.

**Example 5.5.**  $f$  is  $f_{\text{cubic}}$ . Equation (4) with (3) is

$$-c\dot{\phi}(\xi) = \epsilon^2 \ddot{\phi}(\xi) - \phi(\xi)[\phi(\xi) - 1]^2, \quad \text{when } a = 1$$

and

$$-c\dot{\phi}(\xi) = \epsilon^2 \ddot{\phi}(\xi) - [\phi(\xi)]^2[\phi(\xi) - 1], \quad \text{when } a = 0.$$

We consider the  $a = 0$  case, the  $a = 1$  case being similar. Let  $c_* = -\epsilon/\sqrt{2}$  for which we know there exists a connecting orbit between 0 and 1. A simple geometric argument shows that there exists a flow from 1 to 0 for all  $c < c_* = -\epsilon/\sqrt{2}$ , flows that connect a saddle point to a node, a travelling wave, and solutions which turn out to be unstable for (1) to perturbations in the leading tail. For (14) or (13) with (3) the range of  $c$  for which there is a heteroclinic orbit is a subset of  $(-\epsilon/\sqrt{2}, \epsilon/\sqrt{2})$ , as shown in figure 6.

**Example 5.6.**  $f$  is  $f_1$ . Here,  $c_*^2$  is inversely proportional to  $\delta$  for (4) and  $df(\phi, u_0 = a)/d\phi = \delta^{-1}$ . Thus,  $c_*$  is inversely proportional to the slope of the nonlinearity at its middle root.

## 6. Complete discretization—backward Euler and rectangular spatial mesh

In this case, we have a difference equation with no differential terms. Depending on the choice of  $c$ ,  $\Delta t$ ,  $\Delta x_i$ ,  $i = 1, \dots, n$ , and direction  $\sigma$ , the solution  $\Psi$  is either a dense or discrete set of values in  $[0, 1]$ . Suppose all the delays in (15) are rationally related then the solution will be a discrete set of values in  $[0, 1]$  and the domain,  $D$ , is a discrete set of  $\mathbb{R}$ . If any of the shifts is irrationally related, then the domain  $D$  is dense in  $\mathbb{R}$ . In both cases the solution profile contains jump discontinuities. To deal with this, define

$$\Psi_\tau(\xi) = \tau\Psi(\xi^-) + (1 - \tau)\Psi(\xi^+) \quad \text{with } \tau \in [0, 1],$$

and shift the independent variable to obtain

$$-\Psi_\tau(\xi + c\Delta t) + \Psi_\tau(\xi) = \Delta t[\epsilon^2 L_T \Psi_\tau(\xi) - f(\Psi_\tau(\xi))],$$

where  $L_T$  is given in (14). This equation holds for all  $\xi \in \mathbb{R}$  including the values of  $\xi$  where there are discontinuities. Since, typically, wave profiles are thought of as maps  $\varphi: \mathbb{R} \rightarrow \mathbb{R}$  this is how we will define the following solutions and we will discuss the restriction to  $D$  as a remark. The solution profiles will form steps when  $|c| \rightarrow \infty$  and  $|c| \rightarrow 0$ . The difference between the two cases comes from whether the temporal or the spatial discretization dominates the behaviour.

For the cases when  $|c|$  is large we assume  $c > 0$  and  $\Delta t > 0$  (the  $c < 0$  case is similar) and let  $\phi(\eta) = \Psi(\xi)$  with  $\eta = \xi/c$ . Then (15) becomes

$$-\phi(\eta) + \phi(\eta - \Delta t) = \Delta t[\epsilon^2 L_\infty \phi(\eta - \Delta t) - f(\phi(\eta - \Delta t))], \quad (39)$$

where

$$L_\infty \phi(\eta) = \sum_{i=1}^n \left\{ \frac{1}{\Delta x_i^2} \left[ \phi\left(\eta + \frac{\Delta x_i}{c} \sigma_i\right) + \phi\left(\eta - \frac{\Delta x_i}{c} \sigma_i\right) - 2\phi(\eta) \right] \right\}.$$

In [10], nonuniqueness was observed for  $\Delta x_1, \dots, \Delta x_n, \Delta t$  large enough and the shifts  $\sigma_1 \Delta x_1, \dots, \sigma_n \Delta x_n, c \Delta t$  rationally related for the complete discretization with the piecewise linear nonlinearity  $f_{\text{pwl}}(8)$ . This effect also occurs for the nonlinearities  $f_{\text{cubic}}(3)$ ,  $f_1(7)$  and  $f_2(6)$ . Consider the equation

$$\begin{aligned} 0 = & \frac{1}{\Delta t} [\Psi(\xi + c\Delta t) - \Psi(\xi)] + \epsilon^2 \sum_{i=1}^n \frac{1}{\Delta x_i^2} [\Psi(\xi + \sigma_i \Delta x_i) - \Psi(\xi)] \\ & + \epsilon^2 \sum_{i=1}^n \frac{1}{\Delta x_i^2} [\Psi(\xi - \sigma_i \Delta x_i) - \Psi(\xi)] - f(\Psi(\xi), a), \end{aligned} \quad (40)$$

where  $f$  is one of our three example nonlinearities; let  $M(\Delta x_1, \dots, \Delta x_n, \Delta t) = 1/\Delta t + 2\epsilon^2 \sum_{i=1}^n 1/\Delta x_i^2$ , the sum of the coefficients of the difference terms, and recall the continuous function  $h(a)$  in (35), in (37) and in (38), and figures 7 and 8.

**Theorem 6.1.** *For any fixed  $\epsilon^2 \geq 0$  and  $c \in \mathbb{R}$ , if the  $\Delta x_i$ ,  $i = 1, \dots, n$ , and  $\Delta t$  are chosen so that*

- (i)  $M(\Delta x_1, \dots, \Delta x_n, \Delta t) < h(\frac{1}{2})$  and
- (ii) the shifts  $\pm \sigma_i \Delta x_i$  and  $c \Delta t$  are rationally related,

then there exists an interval,  $J$ , of values of  $a$  for which (40) has a nondecreasing discrete solution that connects 0 and 1. Furthermore, for such a set  $\{\Delta x_1, \dots, \Delta x_n, \Delta t\}$ ,  $a \in J$  if  $h(a) \geq M(\Delta x_1, \dots, \Delta x_n, \Delta t)$ .

**Proof.** This result follows directly by applying theorem 2.1 of [22] and by following the procedure for estimating the upper bound of theorem 2.1, found also in [22]. ■

The interval of  $a$  values,  $J$ , associated with a given  $c$  is larger than the interval of values given by theorem 6.1 and the upper bound  $h(\frac{1}{2})$  is overly restrictive.

To illustrate theorem 6.1 consider figure 7. The value  $h(\frac{1}{2})$  is approximately 0.0481 and is the maximum of  $h(a)$ , the shaded area shows the values of  $a$  for which (40) has a solution. For example, suppose we choose the  $\Delta x_i, i = 1, \dots, n$ , and  $\Delta t$  so that  $M = 0.02$  (the horizontal dashed line in the figure). Then, the interval  $J$  contains the interval  $[a_1, a_2]$ .

**Remark.** Although for a particular choice of the parameters  $\epsilon, c, \Delta x_1, \dots, \Delta x_n, \Delta t, \sigma_1, \dots, \sigma_n$  the detuning parameter  $a$  can be set valued, for a particular choice of  $a$ , in the set  $J$ ,  $\Psi(\xi)$  is uniquely determined up to translational invariance.

## 7. Conclusion

In this paper, we have analysed the dynamics of appropriate temporal discretizations and uniform spatial discretization on travelling wave solutions of bistable reaction diffusion equations. Our approach has been that of applying the discretization scheme to the original PDE and then analysing the travelling equations of the semidiscretization or complete discretization.

Stable BDF discretizations ‘speed-up’ the wave. The maximum speed of a travelling wave for the BDF discretized equation increases (in magnitude) from the speed of the travelling wave of the PDE as the value of  $\Delta t$  increases from 0, and although the maximum speed of the wave for the original PDE is finite, the maximum speed of the wave for the BDF discretized equation approaches infinity for  $\Delta t$  finite valued—call it  $\Delta t_{|c| \rightarrow \infty}$ . For  $\Delta t > \Delta t_{|c| \rightarrow \infty}$  travelling waves only exist for  $u_0 \in (u_-, u_+)$  bounded away from  $u_-$  and  $u_+$ . A second critical value of  $\Delta t$  exists, call it  $\Delta t_{\text{step}} (\leq \Delta t_{|c| \rightarrow \infty})$ , where wave profiles for  $\Delta t < \Delta t_{\text{step}}$  are tanh shaped and for  $\Delta t > \Delta t_{\text{step}}$  contain steps along the profile.

Uniform spatial discretization slows down the travelling wave and can stop the wave even though  $\int_{u_-}^{u_+} f(u) \neq 0$ . The maximum speed of a travelling wave for the uniformly spatially discretized equation decreases (in magnitude) from the speed of the travelling wave of the PDE as the value of  $\Delta x$  increases from 0, and the maximum speed (in magnitude) of the wave for the uniformly spatially discretized equation approaches 0 for  $\Delta x$  finite valued—call it  $\Delta x_{|c| \rightarrow 0}$ .

For the cubic  $f$  we have analysed the error in  $(a, c)$  in the limiting case as  $|c| \rightarrow \infty$  (which may be extended to  $|c|$  large), and have found that for complete discretization the  $(a, c)$  curve becomes set valued even for  $c \neq 0$ , implying nonuniqueness in the  $(a, c)$  relationship. Many of the techniques used to analyse the cubic case are also applicable to general smooth bistable nonlinearities. In this work, we assumed that the waveforms for the BDF discretization with cubic  $f$  of (4) are monotone. With some work this is implied by the theory in [3, 23, 24, 31, 32]; see [9].

## Acknowledgments

The work of CEE was supported in part by NSF grant DMS-0204573. The work of ESVV was supported in part by NSF grants DMS-9973393 and DMS-0139824.

## References

- [1] Abell K, Elmer C, Humphries A R, and Van Vleck E S 2005 Computation of mixed type functional differential boundary value problems *SIAM J. Appl. Dyn. Syst.* to be published

- [2] Aronson C G and Weinberger W F 1978 Multidimensional nonlinear diffusion arising from population genetics *Adv. Math.* **30** 33–76
- [3] Chow S N, Mallet-Paret J and Shen W 1998 Traveling waves in lattice dynamical systems *J. Diff. Eqns* **149** 248–91
- [4] Cahn J W 1960 Theory of crystal growth and interface motion in crystalline materials *Acta Met.* **8** 554–62
- [5] Cahn J W, Mallet-Paret J and Van Vleck E S 1999 Traveling wave solutions for systems of ODE's on a two-dimensional spatial lattice *SIAM J. Appl. Math.* **59** 455–93
- [6] Duncan D B and Lynch M A M 1991 Jacobi iteration in implicit difference schemes for the wave equation *SIAM J. Numer. Anal.* **28** 1661–79
- [7] Elmer C E and Van Vleck E S 1999 Analysis and computation of travelling wave solutions of bistable differential-difference equations *Nonlinearity* **12** 771–98
- [8] Elmer C E and Van Vleck E S 2001 Traveling waves solutions for bistable differential-difference equations with periodic diffusion *SIAM J. Appl. Math.* **61** 1648–79
- [9] Elmer C E and Van Vleck E S 2003 Existence of monotone traveling fronts for BDF discretizations of bistable reaction–diffusion equations *J. Dyn. Continuous Discrete Impulsive Syst. A* **10** 389–402
- [10] Elmer C E and Van Vleck E S 2003 Anisotropy, propagation failure, and wave speed-up in traveling waves of discretizations of a Nagumo PDE *J. Comput. Phys.* **185** 562–82
- [11] Evans L C 1998 *Partial Differential Equations (Graduate Studies in Mathematics vol 19)* (Providence, RI: American Mathematical Society)
- [12] Fiedler B and Scheurle J 1996 *Discretization of Homoclinic Orbits, Rapid Forcing and Invisible Chaos* (Providence, RI: American Mathematical Society)
- [13] Fife P C and McLeod J B 1977 The approach of solutions of nonlinear diffusion equations to traveling front solutions *Arch. Ration. Mech. Anal.* **65** 335–61
- [14] Fisher R A 1937 The advance of advantageous genes *Ann. Eugenics* **7** 355–69
- [15] Hairer E and Wanner G 1991 *Solving Ordinary Differential Equations II* (Berlin: Springer)
- [16] Hale J K and Verduyn Lunel S M 1993 *Introduction to Functional Differential Equations* (New York: Springer)
- [17] Heinze S, Papanicolaou G and Stevens A 2001 Variational principles for propagation speeds in inhomogeneous media *SIAM J. Appl. Math.* **62** 129–48
- [18] Hindmarsh A C 1980 LSODE and LSODI, two new initial value ordinary differential equation solvers *ACM-SIGNUM Newslett.* **15** 10–11
- [19] Keener J P 1987 Propagation and its failure in coupled systems of discrete excitable cells *SIAM J. Appl. Math.* **47** 556–72
- [20] Keener J P 1991 The effects of discrete gap junction coupling on propagation in myocardium *J. Theor. Biol.* **148** 49–82
- [21] Keener J and Sneed J 1998 *Mathematical Physiology* (New York: Springer)
- [22] MacKay R S and Sepulchre J-A 1995 Multistability in networks of weakly coupled bistable units *Physica D* **82** 243–54
- [23] Mallet-Paret J 1999 The Fredholm alternative for functional differential equations of mixed type *J. Dyn. Diff. Eqns* **11** 1–48
- [24] Mallet-Paret J 1999 The global structure of traveling waves in spatially discrete dynamical systems *J. Dyn. Diff. Eqns* **11** 49–128
- [25] Nagumo J, Arimoto S and Yoshizawa S 1964 An active pulse transmission line simulating nerve axon *Proc. Inst. Radio Eng.* **50** 2061–70
- [26] Newell A C 1977 Finite amplitude instabilities of partial differential equations *SIAM J. Appl. Math.* **33** 133–60
- [27] McKean H 1970 Nagumo's equation *Adv. Math.* **4** 209–3
- [28] Petzold L R 1982 A description of DASSL: a differential/algebraic system solver *Proc. IMACS World Congress (Montreal, Canada, 1982)*
- [29] Petzold L R 1983 Automatic selection of methods for solving stiff and nonstiff systems of ordinary differential equations *SIAM J. Sci. Stat. Comput.* **4** 136–48
- [30] Stuart A M and Humphries A R 1996 *Dynamical Systems and Numerical Analysis* (Cambridge: Cambridge University Press)
- [31] Weinberger H F 1982 Long-time behavior of a class of biological models *SIAM J. Math. Anal.* **13** 353–96
- [32] Weinberger H F 1979 Genetic wave propagation, convex sets, and semi-infinite programming *Constructive Approaches to Mathematical Models* ed C V Coffman and G J Fix (New York: Academic) pp 293–317
- [33] Zinner B 1991 Stability of traveling wavefronts for the discrete Nagumo equation *SIAM J. Math. Anal.* **22** 1016–20
- [34] Zinner B 1992 Existence of traveling wavefront solutions for the discrete Nagumo equation *J. Diff. Eqns* **96** 1–27